Published in final edited form as:
Biochemistry. 2013 September 3; 52(35): . doi:10.1021/bi400834a.

Use of EPR to Solve Biochemical Problems

Indra D. Sahu, **Robert M. McCarrick**, and **Gary A. Lorigan***
Department of Chemistry and Biochemistry, Miami University, Oxford, OH

Abstract

EPR spectroscopy is a very powerful biophysical tool that can provide valuable structural and dynamic information on a wide variety of biological systems. The intent of this review is to provide a general overview for biochemists and biological researchers on the most commonly used EPR methods and how these techniques can be used to answer important biological questions. The topics discussed could easily fill one or more textbooks; thus, we present a brief background on several important biological EPR techniques and an overview of several interesting studies that have successfully used EPR to solve pertinent biological problems. The review consists of the following sections: an introduction to EPR techniques, spin labeling methods, and studies of naturally occurring organic radicals and EPR active transition metal systems which are presented as a series of case studies in which EPR spectroscopy has been used to greatly further our understanding of several important biological systems.

Keywords

EPR spectroscopy; site-directed spin labeling; naturally occurring organic-based radicals; transition metals; metalloenzymes; ESEEM; ENDOR; DEER

Introduction To EPR-Based Methods

EPR Spectroscopy

EPR spectroscopy requires the presence of an unpaired electron spin. Historically, this has limited the scope of biological systems that could be studied using EPR to those containing organic-based radicals or EPR active transition metals. The advent of spin labeling methods has expanded the technique to include proteins and nucleotides in which an unpaired electron spin can be introduced.[1,2] The simplest EPR active system consists of a single unpaired electron spin residing in a molecular orbital. The electron can exist in one of two M_s quantum states, +½ and -½. In the absence of a magnetic field, these two states are degenerate and have the same energy. However, when a magnetic field is applied, the -½ state decreases in energy and the +½ state increases in energy as a function of the strength of the magnetic field as seen in Figure 1.[3]

The energy separation between the two spin states is $g\beta_e B_0$ where g is a proportionality factor that can be thought of as similar to a chemical shift parameter in NMR, β_e is the electron Bohr magneton, and B_0 is the strength of the static magnetic field. Contrary to NMR studies, where continuous wave experiments have been replaced with pulsed methods, continuous wave (CW) EPR is the most frequently used spectroscopic technique. In a typical CW-EPR experiment, a constant microwave frequency is applied and the B_0 magnetic field is swept with spin-flip transitions occurring when the energy separation between the two electron spin states matches the constant microwave energy. In addition to

*Corresponding Author Telephone: (513) 529-2813, Fax: (513) 529-5715, lorigag@muohio.edu.

sweeping B_0, the field is typically modulated to enhance the signal to noise of the spectra. This gives rise to the derivative lineshape typically observed in most EPR spectra, as it is essentially the slope of the signal that is being measured as the bulk magnetic field is swept and not the signal itself. As depicted in Figure 1, the derivative shaped signal occurs when the separation in energy between the two spin states matches the applied microwave radiation.

The magnetic field at which this signal appears depends on the g value, which dictates the slope at which the energy levels for the two spin states change as a function of the magnetic field. A free electron in a vacuum has a g value (g_e) of 2.00231930436153 (uncertainty 0.00000000000053), which is one of the most precisely known values in physics.[3] Shifts from this value occur due to spin orbit coupling within the molecule. In most biological systems, the g value is anisotropic with an orientation dependence meaning that the effective g value is different depending on the orientation of the molecule with respect to the applied magnetic field.

The EPR spectrum is also dependent on interactions between the electron spin and any NMR active nuclei in the vicinity. This interaction is termed the hyperfine interaction (A) and depends on the amount of electron spin density on the nucleus, the distance between the electron spin and the nucleus, and the angle between the two with respect to the magnetic field. Like the g value, this is also often orientation dependent. Other parameters that can be extracted from an EPR spectrum are electron-electron couplings between two sets of spins that can provide valuable distance information between biological systems and zero field splittings in higher spin systems. The information that can be obtained through the extraction of these parameters will be discussed in the following sections on spin labeled and naturally occurring EPR active systems.

Electron Nuclear Double Resonance (ENDOR) Spectroscopy, Electron Spin Echo Envelope Modulation (ESEEM) and Hyperfine Sub-level Correlation (HYSCORE) Spectroscopic Techniques

In ENDOR, ESEEM and HYSCORE spectroscopies, the electron spin is essentially used as a detector to probe nuclei that are coupled to the unpaired electron spin. With ENDOR, nuclear transitions are directly driven using either continuous or pulsed radio frequency (RF) radiation.[4-7] The effect on the EPR signal as a function of the RF is monitored and what is obtained is essentially an NMR spectrum of the nuclei that are coupled to the unpaired electron spin. Similar to ENDOR, ESEEM and HYSCORE are pulse methods that are used to gain information about nuclei in the vicinity of the unpaired electron spin.[7-11] However, unlike ENDOR, in ESEEM and HYSCORE, nuclear transitions are not directly excited. Instead, the timings between the pulses are varied and the size of either a Hahn or stimulated echo is monitored as a function of time. Similar to the FID signal in an NMR experiment, the time-based data yields a periodic signal dependent on the nuclear Zeeman, hyperfine and quadrupolar (for $I > 1/2$ nuclei) interactions. A Fourier Transform of the time-based data yields a frequency dependent spectrum similar to that obtained in an ENDOR spectrum, but often with double quantum and combination peaks. The most commonly used ESEEM pulse sequences are the two-pulse and three-pulse sequences.[8, 9] HYSCORE is a two-dimensional ESEEM technique in which the peaks are separated into a second dimension, which can often be beneficial for complicated spectra with many overlapping peaks.[11]

Double Electron-Electron Resonance (DEER) or Pulse Electron Double Resonance (PELDOR) Spectroscopy

In systems with two or more EPR active species, there will be an electron-electron dipolar interaction present.[7, 12] This interaction depends upon the distance and the angle between

the two paramagnetic species relative to the externally applied magnetic field. In DEER spectroscopy, that dipolar coupling is measured and as a result, the distance between the two species can be accurately determined between 20 Å - 80 Å.[13] This technique has emerged as a very powerful structural biology tool, particularly for site-directed spin label studies in which the two unpaired electron spins can be engineered into specific locations in biological macromolecules. A more detailed description of DEER studies on spin labeled systems can be found below.

Spin Label EPR

Early biological EPR studies were restricted to those systems containing naturally occurring radicals and EPR active transition metals which will be discussed in a later section. However, with the advent of spin labeling, biological techniques used to place stable radicals at specific locations on biological macromolecules, the potential use of EPR has been extended to nearly any biological system. This is a very broad field of study, and as such, what follows is a basic introduction to the types of experiments and systems in which spin label EPR is being used. For more in depth examinations of this topic, the authors direct the reader to several excellent reviews.[1, 2, 14-19]

The two most widely used techniques for obtaining detailed structural information in biological systems are X-ray crystallography and NMR spectroscopy. These techniques can yield highly detailed structural and in the case of NMR also dynamic information for a variety of biological systems. These methods have their own advantages and limitations. Solution NMR can provide structural information in a physiologically relevant environment, but is limited due to size restrictions (approximately ≤ 50kD).[14, 20-22] NMR structural studies on membrane proteins are also challenging due to the size of the micelle complex and corresponding increases in linewidth.[23] X-ray crystallography yields highly resolved structural information, but cannot provide detailed dynamic information.[24] In addition, the hydrophobic surfaces associated with membrane proteins often complicate the crystallization process, limiting the use of X-ray crystallographic techniques for many membrane protein systems.[21] EPR Spectroscopy has emerged as a powerful technique to overcome these limitations and provide important solutions to getting structural and dynamic information on peptides, proteins, macromolecules, and nucleic acids.[1,2,15,16,25-29]

EPR spectroscopy offers high sensitivity (micromolar concentrations), and is not limited by the size of the protein or the optical properties of the sample. EPR measurements can be made on samples ranging from proteins in solution to densely packed membrane suspensions, tissue samples, ammonium sulfate-precipitated solids, or samples frozen and maintained at cryogenic temperatures.[30] EPR measurements are routinely made from approximately 70 nanoliters of sample at W-band (94 GHz)[31] to several mL of sample or even small animals at L-band (1–2 GHz).[32] EPR spectroscopy can address important structural and dynamic questions related to both solution and membrane embedded protein systems that are not solved by traditional methods.[1, 15, 28, 33] CW-EPR spectroscopy of spin-labeled molecules reveals structural and dynamic information about the motion of the nitroxide side chain, solvent accessibility, the polarity of its surrounding environment, and intra- or intermolecular distances between two nitroxides or a single nitroxide and another paramagnetic center in the system.[27] The analysis of the EPR data for a series of spin-labeled protein sequences allows modeling of the protein structure with a spatial resolution at the level of the backbone.[34-37]

Site-directed Spin Labeling Methods

Most native biological systems cannot be studied with EPR spectroscopy as they are not naturally EPR active. A reporter group or a label such as spin probe needs to incorporated

into the system of interest to be detected by EPR. The site-specific incorporation of unpaired electrons into biomolecules in the form of spin labels is known as site-directed spin labeling (SDSL).[38, 39] In SDSL experiments, all native nondisulfide bonded cysteines are eliminated by replacing them with another amino acid such as alanine. A unique cysteine residue is then introduced into a recombinant protein via site-directed mutagenesis, and subsequently reacted with a sulfhydryl-specific nitroxide reagent to generate a stable paramagnetic EPR active side chain.[27, 39, 40] Figure 2 shows the structure of the most commonly used spin label, MTSL, and the resulting side chain produced by reaction with the cysteine residue of the protein.

EPR Structural And Dynamic Information Of Biological Systems

The EPR spectra of nitroxide-based site directed spin labels are sensitive to the motion of the spin label and as such, can be used to observe dynamics within a system.[1] This sensitivity stems from the orientation dependence of both the g values and the hyperfine couplings and the extent to which they are averaged out by the motion of the spin label. For spin labels that are moving very rapidly in solution, the spectrum collapses to three sharp peaks. Conversely, if the spin label motion is very slow such that it is relatively motionless within the transverse relaxation time for the system, the spectrum is in the rigid limit.[41] In a rigid limit spectrum, it is as if the sample has been frozen and the full orientation dependent parameters are observed. These “book ends” to the spin label spectra are determined by the transverse relaxation time (T_2), which in turn determines the range of motional dynamics for which EPR is sensitive. For systems in which the spin label movement falls between these two extremes, a correlation time, τ_c, can be determined that indicates the dynamic properties of the spin label at a specific location.[41] The overall mobility of the nitroxide spin label attached to the protein or peptide is a superposition of the contributions from (1) the motion of the label relative to the peptide backbone, (2) fluctuations of the α-carbon backbone, and (3) the rotational motion of the entire protein or peptide. Under experimental conditions, these motions can be isolated from the EPR spectrum. The spin label side chain motion is used to study tertiary contacts and protein structure. There are five chemical bonds between the pyrroline ring of the attached MTSL and the α-carbon backbone of the protein (see Figure 2). The flexibility of the MTSL at α-helical sites is dominated by rotations about the two bonds closest to the nitroxide ring moiety (χ_4 and χ_5).[42] The interaction of the disulfide bond with the backbone Cα hydrogen restricts mobility about the first two bonds adjacent to the Cα backbone (χ_1 and χ_2). An isomerization about the disulfide bond (χ_3) is slow on the EPR time scale so that the motion of the MTSL is constrained to isomerizations about χ_4 and χ_5. For β-sheet proteins, the spin label motion is influenced by steric interactions with the nearest neighbors.[43] The inverse linewidth of the central line provides a measure of relative mobility. Scanning the inverse linewidth of the EPR spectrum against the amino acid sequence yields a periodic data profile that reflects the local secondary structure of the protein.[44] This EPR approach has been routinely used to determine the secondary structure of protein and peptides (see review by Klug et al.).[1] This method also provides an efficient strategy for identifying functional domains in high molecular weight proteins, supramolecular complexes and membrane proteins.[24] A more detailed description of sidechain motion of the spin label in a biological system can be obtained with EPR spectral simulations such as the microscopic ordered and macroscopic disordered (MOMD) approach.[42, 43, 45, 46]

An excellent example of the application of SDSL EPR techniques is work done on the Escherichia coli ferric citrate transporter FecA.[47] Outer-membrane TonB-dependent transporters such as the Escherichia coli ferric citrate transporter FecA (Figure 3)[48-50] interact with the inner-membrane protein TonB through an energy-coupling segment called the Ton box. This FecA protein is involved in ferric iron-iron translocation across the outer

membrane. Mokdad et al. determined the position and dynamics of the N-terminal transcriptional domain in FecA using SDSL EPR.[47] X-band CW-EPR spectra were recorded for several single spin-labeled sites to determine the N-terminal transcriptional motif with and without substrate binding. The more ordered regions of the domain yielded the broadest spectra while the loop region yielded the narrower spectra with correlation times on the order of 1 ns. No significant spectral differences were observed with and without substrate binding. These results indicated the correct folding of the N-terminal extension with no change in dynamics upon substrate binding. Further spectral analysis indicated that the domains have significant backbone motion on the nanosecond timescale that would be expected for a domain designed for protein-protein interactions. A further study of ten different spin labeled sites in N-terminal transcriptional domain in the absence and presence of PEG 3350 indicated the existence of a conformational equilibrium at these sites.[47] The position of the N-terminal transcriptional domain is not fully resolved in high-resolution crystal structures of FecA. This study also used DEER distance restraints obtained for pairs of spin labels located on the N-terminal signaling domain and the Ton box or the FecA barrel to determine structure models of the apo, TonB, and substrate-bound states.[47]

Another example of using SDSL EPR to probe the structural and dynamic properties of proteins is Vimentin (Figure 4).[51, 52] Vimentin is a Type III intermediate filament protein found in many cells of mesenchymal origin. The intermediate filament (IF) gene family includes more than 65 different members, each expressed in a cell-specific or differentiation stage-specific manner. Mutations in IF genes have been linked to more than 85 different human diseases.[52] Aziz et al. used site-directed spin labeling X-band CW-EPR data collected at 45 different sites to predict the structural model of the Vimentin head domain.[52] This study also revealed that the Vimentin head domain structure is dynamic and changes with the filament assembly. Hess et al. further employed X-band CW-EPR to show that the head and tail domains of Vimentin are structurally very different and the tail domain undergoes distinctive conformational changes upon assembly with the tetrameric protofilament.[51]

Protein Topology

Membrane proteins play an essential role controlling bioenergetics, the movement of ions across a cell, and initializing signaling pathways. Membrane proteins can be incorporated into a membrane in several different fashions or orientations. The embedded helices may be short, long, kinked, or interrupted in the middle of the membrane. They may cross the membrane at different angles, lie flat on the surface of the membrane or form re-entrant loops. Nitroxide-based site-directed spin labeling EPR can be used to achieve pertinent structural and dynamic information on membrane-protein assembly. EPR spin labels are very sensitive to the presence of other paramagnetic species which alter the relaxation properties.[53] The accessibility of the spin label to different paramagnetic probes can be used to determine the location of the spin label in the membrane interior. EPR power saturation experiments can monitor the relaxation rate of spin labels with extrinsic paramagnetic probes residing in the aqueous phase and in the lipid bilayers by examining the EPR signal intensity as a function of microwave power.[54] The power at which the measured signal amplitude is half-saturated, $P_{1/2}$ is proportional to the longitudinal relaxation rate of the spin label. When the spin label is exposed to paramagnetic reagents, the spin lattice relaxation rate increases, which is dominated by Heisenberg spin exchange.[54] The most commonly used paramagnetic agents in EPR accessibility experiments are lipid soluble oxygen which serves as a probe for membrane insertion and polar Nickel compounds such as nickel (II) ethylenediaminediacetate (NiEDDA) which is located in the aqueous phase. Nitrogen is used as a control to purge the sample of oxygen during the measurement of the natural longitudinal relaxation rate of the spin label. There are several biologically important

membrane protein systems (e.g. Bacteriorhodopsin, ABC cassette transporter MsbA, Cytochrome C oxidase subunit IV (COX IV) and Ferric enterobactin receptor FepA) that have been studied using spin labeled EPR spectroscopy to investigate structural topology.[54-58] Given the limited format of this review, we are presenting a few recent examples from several studies that are biologically important.

A recent example of using CW-EPR power saturation data is to study the topology of the KCNE1 membrane protein in proteoliposomes.[59] KCNE1 (Figure 5)[60] is a single transmembrane protein that modulates the activity of the KCNQ1 voltage gated potassium channel. EPR power saturation data revealed that KCNE1 spans the full width of the lipid bilayer with Leu59 residue located near the center of membrane. Additionally, SDSL EPR lineshape analysis showed that the dynamic motion of the nitroxide spin-label is slower in the membrane environment than in micelles and that residues within the membrane are less mobile than that outside. This information provides an understanding of how KCNE1 is stabilized in a more native membrane environment when compared to micelles.

The accessibility parameters obtained for a series of consecutive sites can also be used to probe the secondary structure.[1] The plot of accessibility parameters against residue number can distinguish α-helical, β-strand, and unstructured regions of a protein. A standard α-helix has a periodicity of 3.6 residues per turn, so every 3 or 4 residues would be highly exposed to the solvent showing high NiEDDA values, while the sites on the other side of the helix would be buried against the protein revealing lower values for both NiEDDA and Oxygen. Similarly, the β-strand has a periodicity pattern of 2, when compared to a standard α-helix.

An excellent example of using both accessibility data and mobility data to identify the α-helical secondary structure is a study on the lactose permease protein.[61] The X-ray crystal structure of wild-type lactose permease protein is shown in Figure 6.[62] Voss et al. used site-directed spin labeling EPR to obtain the periodicity of side chain mobility and accessibility to molecular O_2 and concluded that the transmembrane domain XII in the lactose permease protein adopts an α-helical conformation.[61] For integral membrane proteins, the depth of a given spin label side chain within a lipid bilayer can be determined using accessibility data based on the inverse concentration gradients of oxygen and NiEDDA within a lipid bilayer.[54, 59]

CW-EPR spectroscopy at X-band can also be used to study membrane topology of integral membrane proteins inserted into aligned phospholipid bilayers.[63] Recently, Ghimire et al. used the membrane alignment technique coupled with dipolar broadening CW-EPR to determine the distance and relative orientation of two nitroxide spin labels on the M2δ peptide of the acetylcholine receptor (AchR) in DMPC vesicles.[64]

High Field/High Frequency SDSL EPR Methods

EPR spectral lineshape can provide information on the secondary structure of a protein and on the orientation of its subunits relative to each other or to the environment. If the experiment is performed at more than one frequency, it can provide additional information about both the global tumbling of the protein and the internal motion consisting of backbone fluctuations and side chain isomerizations.[65, 66] EPR spectral behavior at lower frequency is more sensitive to slower spin motions, whereas spectral behavior at higher frequency is more sensitive to faster spin dynamics.[67] A multi-frequency approach supplies snapshots at different time-scales, but also provides pertinent information from a different angle: hyperfine tensor at lower frequencies and g-tensor at higher frequencies. Single frequency spectra can be fit quite easily due to the few parameters that are needed in the EPR spectral simulation. However, EPR spectra collected at multiple frequencies provide unique perspectives on the molecular motions, and therefore taken together provide a more

complete and accurate description of the dynamics of the spin probe environment.[66] The following three major challenges arise for EPR as a biophysical tool, that cannot be resolved by traditional structural methods: 1) structure and dynamics of large molecular weight proteins in solution; 2) membrane and membrane-associated proteins: structure, location with respect to the membrane, side-chain dynamics, and interactions with other membrane components or DNA or RNA; 3) fast conformational transitions of proteins and RNA's in solution, protein folding and refolding. These issues can be more accurately addressed by probing EPR at multiple and higher microwave frequencies.[67] Extending conventional EPR frequencies (X-band) to higher frequencies, the following five important features emerge:[68] 1) enhanced spectral resolution, 2) enhanced orientational selectivity in disordered samples, 3) enhanced low-temperature electron spin polarization, 4) enhanced detection sensitivity for restricted-volume samples, and 5) enhanced sensitivity for probing fast motional dynamics. At magnetic fields above 3.4 T (95 GHz, W band), the rhombic Zeeman term provides new information on protein structure and dynamics which are inaccessible by traditional means.[67] At a frequency of 250 GHz, the slow overall tumbling of large biomolecules is frozen out on the EPR time scale leaving only the rapid internal modes corresponding to backbone fluctuations in spin-labeled proteins to contribute significantly to the EPR spectrum.[65, 69] The additional advantages of extending conventional X-band EPR (9 GHz) to high frequency EPR include an increased signal-to-noise ratio and a great improvement in orientational resolution of the nitroxide spectrum.[69] More detailed information on the application of high field EPR to study biological systems can be found in the literature.[70, 71] The following are recent examples of such multi-frequency studies.

Multi-frequency EPR spectroscopy has provided pertinent structural and dynamic information on myosin.[72] Myosins are a family of ATP-dependent motor proteins. They are involved in muscle contraction and a wide range of other eukaryotic motility processes. An X-ray crystal structure of the motor domain of Dictyostelium discoideum myosin II is shown in Figure 7.[73] Nesmelov et al. recorded CW-EPR spectra at X- and W-band frequencies on spin labeled subfragment 1 (S1) of rabbit skeletal myosin for the apo state and in the presence of ADP and nucleotide analogs.[72] Using simultaneous frequency data fits, both the rate and amplitude of restricted motion within myosin were determined and multiple conformational states were resolved in the force generating region of myosin. This study also provided reliable information about the allosteric influence of nucleotides on multiple conformational states, the relative populations of these states, and the rate and amplitude of spin label rotation in each state.[72] This study further suggested that the post- and pre-powerstroke structural states are in a dynamic equilibrium in solution, even with ADP and vanadate tightly bound to the myosin active site. The molecular events responsible for force generation in a cycling cross-bridge are a major focus of interest in the muscle field.[74] This important study provided the pertinent structure and dynamic information on the force generating domain of myosin, addressing a major focus of interest in the field.

Multi-frequency EPR has also been used to study the dynamic properties of T4 lysozyme in solution.[66] T4 lysozyme is a globular protein composed of 164 amino acid residues with a molecular weight of 18.7 kDa.[66] Zhang et al. used EPR spectroscopy over a wide range of frequencies (9, 95, 170, and 240 GHz) to obtain dynamic modes of nitroxide side chains in T4 lysozyme.[66] This study demonstrated the power of multi-frequency EPR to differentiate the effects of faster internal modes of motion from slower overall motions.

SDSL-ESEEM Methods

Electron Spin Echo Envelope Modulation (ESEEM) spectroscopy is a very powerful pulsed EPR spectroscopic technique and has been applied to study many different biological systems.[75-79] ESEEM can provide distance measurements up to 8 Å between a spin label and a single ^{2}H nucleus. Simulations of the spectral data can indicate the number, identity,

and radial distance of the weakly coupled nuclei from the electron spin.[7, 80] Volkov et al. used ESEEM accessibility data to measure the folding kinetics of the plant light harvesting complex LHCII membrane protein in a membrane environment.[78] Recently the Lorigan lab has utilized ESEEM spectroscopy to directly probe the site-specific secondary structure of membrane peptides using microgram amounts of sample.[77, 81, 82] In this method, a cysteine mutated nitroxide spin label is positioned 2 (i+2), 3 (i+3), or 4 (i+4) residues away from a fully deuterated Leu chain (i). The characteristic periodicity of the α-helical and β-sheet structure gives rise to a unique pattern in the ESEEM spectra. For i+2 α-helix samples and i +3 β-sheet samples, the ^{2}H nuclei are too far away to be detected. However, with the 3.6 residue per turn pattern of an α-helix, the *i+3* samples reveal a strong ^{2}H ESEEM peak from ^{2}H nuclei of the Leu side chain weakly-coupled to the spin label. Similarly, the i+2 sample for a β-sheet can reveal an ESEEM signal from ^{2}H nuclei of the Leu side chain coupled to the spin label because they are in close proximity. This method is very simple and quick (less than an hour) to discern the local secondary structure within a protein. Figure 8 shows an example of the three-pulse ESEEM data obtained for AchR M2δ α-helical peptide in a membrane environment and an ubiquitin β-sheet peptide in solution.[77]

Double Site-directed Spin Labeling Methods for Distances

One of the most active and rapidly developing aspects of EPR spectroscopy is the measurement of distances between two spin labels in the terms of either intramolecular distances on the same protein or intermolecular distances between sites on different proteins.[30] The distance is obtained from the magnetic dipolar interactions between the unpaired electrons of two spin labels or a spin label and a paramagnetic metal. Using dual labeling EPR techniques, distances can be measured to probe secondary, tertiary and quaternary structures.[30] This method allows the relative orientations between interacting spin labels to be determined from CW-EPR studies in those cases where a specific orientation exists.[31] The magnetic dipoles of the two spin labels give rise to a distance dependent line broadening in the conventional CW-EPR spectrum. CW dipolar broadening EPR can provide pertinent structural and functional dynamic information over an intermediate distance range of 8-20 Å.[83] Recently, the Hyde group extended the upper limit distance measurement to 30 Å at L-band (1-2 GHz) using non-adiabatic rapid sweep electron paramagnetic resonance (NARS EPR).[84] For higher resolution structure analysis, quantitative distances can be determined using spectral simulations.[31, 85-87] The resolution of this method is typically on the order of ± 1-2 Å for flexible spin labels and 0.1-0.2 Å for highly immobilized, well-oriented spin labels.[31]

The CW-EPR line broadening approach has been used to study the bacterial K^+-translocating protein KtrB.[88] Proteins of this superfamily of potassium transporters are found in archaea, bacteria, fungi, plants and trypanosomes. They are involved in the uptake of K^+ and Na^+ by the cells. CW-EPR dipolar broadened data obtained for double-labeled variants of KtrB in the presence and absence of K^+ ions have provided valuable structural models for the open and closed state conformations.[88]

For longer distances, pulsed DEER spectroscopy has proven to be a very powerful and popular structural biology technique for measuring longer range distances (20-80 Å).[13, 89] In DEER, one set of spins are monitored and another set of spins are excited with a second microwave frequency leading to the measurement of the coupling between the two spins and thus the distance between them. DEER can probe the structure of biomacromolecules, globular proteins, membrane proteins, oligomerization states, and RNA.[13, 89-94] In addition to measuring distances, DEER at high field can be used to measure the relative orientation of the spins.[95] DEER provides long range structural distance constraints of the protein backbone and information on conformational mobility in specific loop regions.[96] However, in some cases, the high effective concentration in the two-dimensional environment of

membrane systems develops a strong background contribution imposing severe limits on sensitivity, distance range and experimental throughput.[97] Recent studies have reported an increase in sensitivity in DEER measurements for proteins when the experiment is performed at Q-band when compared to X-band.[98-101] Also, Hubbell and coworkers have used a rigid nitroxide side chain RX to minimize the spin label motion for more accurate distance measurements.[102] The RX side chain can be generated by a facile cross-linking reaction of a bifunctional methanethiosulfonate reagent with pairs of cysteine residues at i and i + 3 or i and i + 4 for an α-helix, and at i and i + 2 for a β-strand, or with cysteine residues in adjacent strands in a β-sheet. The protein fluctuation dynamics and spin label rotameric motions have a significant contribution to the DEER distribution width. With the development of molecular dynamics simulations, recently Jao et al.[103] and Hirst et al.[104] have used DEER distance restraints to refine the secondary structure of membrane associated proteins. These methodological developments have made DEER, a powerful spectroscopic tool to solve several pertinent biological problems.

DEER has been used to identify the curved α-helical nature of the transmembrane region of the C99 Amyloid Precursor Protein in proteoliposomes as shown in Figure 9.[105] C99 is a transmembrane carboxyl-terminal domain of the amyloid precursor protein that is cleaved by γ-secretase to release amyloid-β polypeptides which are involved in Alzheimer's disease. Two MTSL spin labels were generated at the ends of the transmembrane domain (TMD) of C99 (700-723). The dual spin labeled C99 protein was reconstituted into LMPG micelles and POPC/POPG liposomes. The distance distributions were obtained by analyzing the time evolution DEER data. The identical distances obtained for both LMPG micelles (33.5±1.2 Å) and POPC/POPG liposomes (34.5±0.5 Å) verify that the TMD attains similar curvature in liposomes and in micelles. The curved nature of the TMD is very important for C99 interactions with γ-secretase. Additionally, CW-EPR power saturation data were used to conform the spanning of TMD of C99 and revealed that the N- and C-helices are associated with the membrane surface.

Another recent example using SDSL/EPR distance methods is on the cardiac Na^+/Ca^{2+} exchange (NCX1.1) system.[106] The cardiac Na^+/Ca^{2+} exchange protein is an antiporter membrane protein that removes calcium from cells. The exchanger is regulated by binding of Ca^{2+} to its intracellular domain, which contains two homologous Ca^{2+} binding domains (CBD1 and CBD2). NMR and X-ray crystallographic studies have provided the structures for the isolated CBD1 and CBD2 domains and the corresponding effect of Ca^{2+} binding on their structures and motional dynamics. However, structural information was not obtained on the entire Ca^{2+} binding domain (CBD12) and the effect of Ca^{2+} binding on its structure and dynamics. These questions were addressed using SDSL EPR methods.[106] EPR measurements on singly labeled constructs of CBD12 were used to identify the regions that undergo dynamic changes upon Ca^{2+} binding. DEER measurements on a dual-labeled construct of CBD12 indicated that the β-sandwich regions of the CBD1 and CBD2 domains are widely separated at their N and C termini and are largely insensitive to Ca^{2+} binding. Additionally, the authors used DEER distance restraints to construct structural models for CBD12 in the absence and presence of Ca^{2+}.[106] These structural models indicated that there is not a major change in the relative orientation of the two Ca^{2+} binding domains as a result of Ca^{2+} binding in the NCX1.1 isoform.

Another excellent example for measuring distance constraints with DEER spectroscopy is the Na^+/Proline Transporter PutP *Escherichia coli* system.[107] Na^+/Proline Transporter PutP of *E. coli* is a prokaryotic member of the sodium solute symporters (SSS) family. Proteins of this family utilize a sodium motive force to drive uphill transport of substrates such as sugars, amino acids, vitamins, ions, myo-inositol, phenyl acetate, and urea. A secondary structure model of Na^+/Proline Transporter PutP of E. coli (Figure 10) has been predicted

based on a gene fusion approach, Cys accessibility analysis, site-directed spin labeling, and site-specific proteolysis.[108-110] Hilger et al. used SDSL DEER distances to determine the backbone structure of the transmembrane domain IX of Na^+/Proline Transporter PutP of E. coli.[107] Transmembrane (TM) domain IX appears to line the translocation pathway and is involved in ligand binding and transport. DEER distance distribution measurements for 16 pairs of spin labels were used in helix-loop-helix modeling to predict the kinked helical structure models of TM domain IX of PutP. The kink in the TM domain is associated with a hinge that allows the protein to open and close during substrate binding.[107] DEER has also been successfully used to study the tetrameric potassium ion channel KcsA to measure pertinent distances and the orientation of the spin label.[111] The examples discussed above clearly show the power of SDSL DEER techniques to answer significant biological problems.

Protein-protein Interactions

Protein–protein interactions are involved in almost all biological processes such as immune responses, cell signaling, translocation, and regulation.[112] EPR spectroscopy is a powerful technique to study protein-protein interactions and oligomerization states.[1, 113] When a spin-labeled molecule is mixed with its binding partner, the EPR spectrum constitutes a linear combination of spectra representing the bound and unbound components. The fraction of each state can be extracted by the numerical decomposition of the spectrum.[113] DEER spectroscopy has emerged as a very powerful tool to measure distance between two spin labeled binding sites in a protein-protein complex.[114, 115] A detail application of site-directed spin labeling EPR for studying protein-protein interactions can be found in previous reviews.[1, 14]

A recent example of the application of CW-EPR and DEER spectroscopy to study complicated protein-protein complexes is the interaction of cdb3/AnkD34 proteins.[114] The ankyrin family of adaptor proteins serves critical functions in cells by linking the lipid bilayer to the spectrin-actin-based membrane skeleton as well as assembling proteins in specialized membrane domains. CW-EPR and DEER spectroscopy were used to map the binding interfaces of these two proteins in the complex and to obtain inter-protein distance constraints to build a structural model.[114] Another good example is the ATP-binding cassette transporter in association with antigen processing (TAP), which participates in the adaptive immune defense against infected or malignantly transformed cells. This system translocates proteasomal degradation products into the lumen of the endoplasmic reticulum for loading onto MHC class I molecules. Herget et al. used CW-EPR spectroscopy to reveal conformational details of the bound peptides, and DEER spectroscopy to determine distances in dual-labeled peptides bound to TAP.[116] Also, James et al. used saturation transfer electron paramagnetic resonance (ST EPR) spectroscopy to probe the homo- and hetero- oligomeric interactions of the sarcoplasmic reticulum Ca-ATPase (SERCA) and phospholamban (PLB).[117]

Unpaired Spins in Biological Systems

Many systems in nature contain unpaired electron spin and as such can be studied natively using EPR methods. These systems range from enzymes that function via transient radical intermediates to those containing stable unpaired electron spins and transition metals. Since the electrons being observed often participate intimately in biological processes, EPR methods can reveal pertinent structural information for these systems. In this section, owing to the significant overlap of EPR techniques used to examine naturally occurring radicals and transition metals, we survey selected examples of organic radical-based and transition

metal-based systems that offer illustrative examples of the biological questions that can be answered using EPR spectroscopy.

Naturally Occurring Radicals

Throughout nature, organic based radicals are utilized in enzymatic reactions and electron transport. Some can be persistent, like the tyrosine residue (Y_D) in Photosystem II, but most cycle as part of the function of the system and as such can be short lived. The most common biological radicals are those stemming from amino acid residues such as tyrosine and tryptophan, cofactors such as flavins, and pigment molecules such as chlorophylls.[118] These systems typically contain one unpaired electron spin residing most often in an aromatic molecular orbital. Organic systems containing one unpaired electron spin rarely have g values that deviate substantially from that of a free electron and as such, at the most common frequency used in EPR, X-band (9 GHz), the EPR spectra are typically dominated by hyperfine interactions. Because of this, it can often be difficult to resolve any small orientation dependence that is present in the g values using typical EPR spectrometers. However, access to higher field/frequency instruments is becoming more common and as such, these small anisotropies in the g values are being determined more frequently.[118, 119] The deviation of the g values can be characteristic for a given system and as such, they can be used to gain information on the identity and environment of the electron spin. In cases where the g values can be resolved, the span and skew for the spectrum can be determined based on the canonical g values. These values give the breadth and overall symmetry of the signal.[118] The various commonly observed biological radicals give relatively characteristic values and as such, the high field EPR spectrum can indicate the origin of a radical where a typical X-band EPR spectrum would not be able to resolve any g values rendering these different radical systems indistinguishable. In the following sections, we will show several illustrative examples of how EPR and related methods have been used to answer important biological questions in systems containing organic-based biological radicals. For a more extensive treatment of this topic, we refer the readers to a recent review from Stefan Stoll.[118]

Phycocyanobilin-Ferredoxin Oxidoreductase (PcyA)

Phycocyanobilin: ferrodoxin oxidoreductase (PCYA) catalyzes the reduction of biliverdin to 3Z/3E-phycocyanobilin via a 4 electron process.[119-121] The conversion of biliverdin to a variety of other compounds that have wide ranges in light absorption profiles allow cyanobateria to capture a greater range of light compared to plant systems. This system functions via a two-step, four electron reduction with 181,182-dihydro-biliverdin (DHBV) as the intermediate in the reaction. It was shown that this process proceeds via short-lived radical intermediates (on the timescale of minutes) and that long lived, stable radical intermediates could be produced with certain mutations near the active site of the enzyme. Since no significant DHBV was detected in these mutant systems, it was likely that the intermediate trapped corresponded to the one electron reduced the biliverdin intermediate.[119-121]

As mentioned above, the small amount of g anisotropy present in many biological radicals precludes precise determination of the g values by conventional low field/frequency EPR. Such is the case for the radical intermediate in the PCYA reaction as can be seen in Figure 11. The X-band (9.6 GHz) EPR spectrum of the PCYA intermediate is very nearly isotropic. However, at D-band (130 GHz) the signal is axial with poorly resolved g_x and g_y values. At a very high field and frequency (406 GHz), the signal is still somewhat axial, but the g_x and g_y values show greater separation. A simulation of the high field spectrum was able to extract the three principle g values with a great deal of certainty. While these results are informative, they do not yield information regarding the orientation of these g values with

respect to the molecular frame. To elucidate the orientation of the g values, the researchers underwent a series of single crystal rotation experiments. In these experiments, collected at D-band, three samples were prepared each aligned along one of the principle crystallographic axes. Successful simulation of the data determined the orientation of the principle g values in relation to the molecule frame. With the g values and orientation in hand, the researchers underwent a series of density functional experiments using all possible protonation states for the radical intermediate. Density functional calculations use a quantum mechanical approach to determine a molecular orbital model from a particular basis set and molecular structure. This quantum mechanical model can help predict the EPR parameters such as hyperfine couplings and the magnitude and orientation of the principle g values. The primary factor that gives rise to deviations in g values away from that of the free electron value is spin orbit coupling within the molecule. Spin orbit coupling is the interaction between the unpaired electron spin and low lying unoccupied excited states. Spin orbit coupling for a given degree of electron spin density on an atom increases as the atomic number increases and as such, oxygen atoms within a molecule typically dominate the spin orbit coupling in organic biological radicals. When the predicted parameters from these calculations were compared with the values obtained from the high field and single crystal EPR studies, it was determined that the radical intermediate in the reaction was likely protonated at both the A and D-ring carbonyl oxygens. This prediction carried with it mechanistic implications. The suggested protonation states consistent with the EPR data suggest a proposed mechanism in which one of the intermediates in the first two-electron reduction step consisted of a cationic radical with both terminal oxygen atoms in a protonated state. This study offers a powerful example in which the combination of EPR techniques has shed light on the chemical mechanism of an important biological system.[119]

Ribonucleotide Reductase

Perhaps the most well characterized naturally occurring radicals (tyrosine, tryptophan and cysteine) are those in the various forms of the Ribonucleotide Reductase (RNR) family of enzymes.[122] The RNR family of enzymes catalyzes the conversion of ribonucleotides to the deoxyribonucleotides that are used in the synthesis of DNA in every living organism. In this review we will focus on the Class 1 RNR systems which consist of two subunits, R1 and R2. The ribonucleotide reduction reaction is thought to proceed via the creation of a tyrosine radical in the R2 subunit by the di-iron center in the R1 subunit, followed by an electron transfer reaction creating a thyil radical near the substrate binding site and the subsequent reduction of the ribonucleotide.[123] This radical was first identified not by the high field methods described above, but by monitoring the change in the EPR signal following the isotopic ^{2}H labeling of the β proton positions of the tyrosine residues in the system.[124, 125] At the time, high field EPR instruments were not common and as such, a detailed analysis of the signal was not conducted until years later. As in the case of the PCYA system discussed above, eventually, EPR examinations of this system have benefited greatly from high field/frequency investigations.[126-128] High field single crystal EPR methods were used to determine both the precise canonical g values, and the orientation in crystals that had been soaked in H_2O_2 to generate the radical intermediate (Figure 12).[127] The results showed that the tyrosyl group was tilted slightly when compared to the results from the resting state crystal structure suggesting that the formation of the radical is accompanied by the loss of a hydrogen bond and a shift of the position of the residue that could prove to be critical in the shuttling of hydrogen atoms to and from the residue.[127]

In addition to the information that the g values have provided, the determination of the various hyperfine interactions within the tyrosine radical has yielded insight into the function of the system. The two β protons of the tyrosine radical in RNR have isotropic hyperfine interactions that are sensitive to the dihedral angle of that position in the molecule

and as such have been a good reporter of structure. These hyperfine interactions are difficult to resolve in the EPR spectra, however, they can be directly observed by techniques such as ENDOR. The examination of these hyperfine interactions led to the discovery that several RNR enzymes from different organisms show a variance in the hyperfine pattern for these two β protons. Differences in these hyperfine couplings have correlated with differences in the allosteric regulation of the various classes of RNRs. This suggests varying local structures for the tyrosine radical might have important implications for tuning the reactivity of the enzyme.[129]

Other Important Biological Systems

While the short format of this review precludes a significant overview of the literature, we would like to mention several other systems in which EPR has been used to help solve pertinent biological problems. Quinone-based electron transport systems have been extensively studied using EPR and ESEEM and these studies have helped shed light on the important Q-cycle in the Complex III family of membrane bound electron transport systems.[130] EPR methods have also been used to further the understanding of the roles of the two redox active tyrosine residues within Photosystem II[131]. Many biological cofactors have also been studied using EPR such as chlorophylls, flavins and others.[118]

Metals in Biological Systems

Each year, more and more biological systems are discovered that depend on metals for proper function. These metals can play structural roles, but more often participate in redox reactions and electron transfer. As in the previous section, this topic could easily fill a textbook. As such, we will focus on several illustrative examples in which EPR was used to answer difficult questions in metalloenzymes.

The Oxygen Evolving Complex (OEC) in Photosystem II (PSII)

Photosystem II is a multi-subunit membrane associated enzyme system which catalyzes the light-driven oxidation of two molecules of water to molecular oxygen, releasing four protons that help fuel the pH gradient that drives ATP synthesis, and four electrons in the form of reducing equivalents that eventually participate in the reduction of carbon dioxide to sugar. This reaction proceeds in a light driven fashion where the absorption of individual photons causes the stepwise oxidation of the OEC and the concomitant release of molecular oxygen. The pattern of this cycle was first described by Kok as a series of five “S” states in which S_1 is the dark stable state and S_4 spontaneously decays to S_0 releasing oxygen. The water oxidation chemistry occurs at the OEC which consists of four Mn atoms and one atom each of calcium and chloride (Figure 13).[132, 133]

In the early 1980s, an EPR signal was discovered in chloroplast membranes that had been exposed to a single high-intensity laser flash.[134, 135] The multiline signal (g = 1.96) consisted of approximately 16 hyperfine lines and was similar to that which had been observed in Mn dimer compounds with bridging oxygen ligands. While it was known that the Mn within the system was essential for water oxidation, the similarity of this light-induced spectrum with that of dinuclear Mn compounds shed light on the possible structure of the cluster. The ground state of the species in the S_2 state that gives rise to the multiline signal was determined to arise from an S=½ ground state, meaning that the coupling of the Mn atoms within the cluster was such that there was only one net unpaired electron in the ground state molecular orbital. The span of the spectrum, when compared to the Mn model compounds suggested that there was possibly more than two Mn ions giving rise to the multiline signal. In addition to the multiline signal, a second signal at g = 4.1 was discovered that arose from a separate $S = {}^{5}/_{2}$ species.[136-139] The discovery and analysis of hyperfine lines in the g = 4.1 signal in the presence of ammonia suggested that all four Mn atoms

participated in both the g = 4.1 signal and the multiline signal and suggesting that the two signals stemmed from two separate electronic states of the OEC that were in equilibrium.[140] It has recently been suggested that this interconversion between the multiline and g = 4.1 signals could involve a shift within the bridging oxygens of the OEC from one Mn to another.[141]

Several years later, another multiline signal was discovered that was associated with the S_0 state of the OEC.[142, 143] Like the signal associated with the S_2 state, this signal was centered near g = 2 and had an appearance similar to Mn dimer compounds. The presence and appearance of these two multiline signals, separated by two laser flashes lent a great deal of evidence for Mn centered oxidation on the S_0-S_1 and S_1-S_2 transitions as well as the potential oxidation states of the Mn within those states.

In addition to the traditionally detected perpendicular mode EPR signals discussed above, a signal was discovered for the S_1 state in parallel detected EPR experiments.[144] Parallel mode EPR has different selection rules and as such, can detect transitions which perpendicular mode EPR cannot. It's typically used to observe integer spin systems that would otherwise be EPR silent. This signal was again shown to arise from the OEC based on observed hyperfine interactions.[145] In all, each of the S states with the exception of S_3 and S_4 (which has not been trapped owing to its short-lived nature) have been characterized by EPR spectroscopy with insight into the nature of each of the catalytic steps gleaned from the data.

While EPR spectra can sometimes detect interactions between an unpaired electron spin and other electrons and nuclei in the vicinity, those interactions are often lost in the large inhomogeneously broadened EPR spectra of transition metal systems. To observe these interactions, it's often necessary to use more sophisticated pulse and CW-EPR methodologies. Several of these methods have been very useful for examining the environment of the OEC, particularly ESEEM and ENDOR.

The multiline signal associated with the S_2 state of photosystem II has been investigated with ^{55}Mn ESE-ENDOR.[146, 147] The pattern of the multiline signal arises from the coupling between the S = ½ electron spin and all of the nuclei in vicinity with the isotopically prevalent ^{55}Mn I = $^5/_2$ nucleus being the dominant interaction. Coupling to the four Mn atoms within the cluster gives rise to 1296 (6^4) potential transitions at a given orientation. This is further complicated by the anisotropy in the g tensor and the hyperfine parameters for each of the four Mn nuclei. These essentially infinite number of transitions overlap giving the relatively information poor lineshape which consists of 18-20 features. As such, the interpretation of this spectrum led to several sets of hyperfine parameters that each adequately fit the experimental data, each having different consequences for the electronic and chemical structure of the OEC.[148-150] In an impressive set of experiments, the Britt laboratory removed the ambiguity in these various parameter sets by conducting a series of high frequency ^{55}Mn ENDOR experiments. The hyperfine coupling between the unpaired electron spin and the four Mn atoms is quite strong and much larger than the ^{55}Mn Larmor frequency at X-band. This means that in the ENDOR spectrum, the appearance will be dominated by the hyperfine interaction with peaks occurring at half the hyperfine coupling. This gives rise to the ENDOR spectra shown in Figure 14. These spectra allowed the simultaneous fitting of both the relatively information poor CW-EPR spectra along with the ^{55}Mn ENDOR spectra. While there were multiple interpretations that could adequately fit the CW-EPR spectra, only one of the sets of values also fits the ^{55}Mn ENDOR spectrum. When combining the hyperfine coupling pattern (factoring in the projection factors based on the oxidation states of the Mn) and the J couplings between the antiferromagnetically coupled oxo bridged Mn atoms, the researchers came up with a proposal of a strongly

coupled trinuclear core with a third more weakly coupled Mn and the possible arrangements of the oxidation states of the Mn within the cluster. These interpretations were verified when crystal structures emerged with a rough trimer-monomer pear shape to the electron density.[151] This study demonstrated the powerful potential of EPR to yield structural information for complicated multinuclear clusters. Recently, a higher field ^{55}Mn ENDOR study has been conducted in both the S_0 and S_2 states with structural implications discussed in light of a recent high resolution crystal structure.[152]

In addition to the studies mentioned above, ESEEM and ENDOR techniques have been very powerful in determining ligand identity to the OEC. Through ^{15}N-labeled labeled ESEEM experiments, it was shown before any crystal structures were present that a histidine residue was directly ligated to the cluster.[153, 154] Further experimentation over the years involving multifrequency ESEEM studies has shed light on the hyperfine couplings of the directly bound and second nitrogen of the imidizole ring and the nature of the histidine ligation to the OEC.[155-157] More recently, controversy as to whether or not the C-terminal end of the D1 protein was directly ligated to the OEC was settled with EPR methods. Detection of a ^{13}C coupling in samples prepared with alanine ^{13}C labeled at the carboxylate position lent direct evidence to the many FT-IR examinations that had suggested this ligation.[157, 158] In addition, preparing samples with ^{2}H-labeled water or ^{17}O-labeled water has enabled EPR to determine how many waters are bound at the various states within the S cycle.[159, 160] Careful analysis and simulation of the ENDOR and ESEEM data of PSII poised in the S_2 state with ^{1}H or ^{2}H-labeled water led to the suggestion that one water molecule was likely directly ligated to the cluster with a second at a longer distance, possibly ligated to the Ca within the OEC.[159]

The FeMo cofactor of Nitrogenase

Nitrogen fixation is the process by which N_2 is reduced to two molecules of ammonia and is catalyzed by an enzyme system known as Nitrogenase. This system consists of two parts, an electron delivery system, the Fe protein, which delivers an electron upon the hydrolysis of two molecules of ATP and the second part, the FeMo protein which contains an iron-molybdenum cluster where the catalysis takes place.[161, 162] Figure 15 shows the X-ray crystal structure of FeMo cofactor of Nitrogenase.[163] Despite intense work for decades, there are still many unanswered questions for this complex system. However, EPR methods have shed light on a lot of what is known about this system. As with PSII, many of the intermediate states have EPR spectra which by themselves are informative and also allow techniques such as ENDOR to be used to further characterize the system. There are a large number of EPR spectra that have been generated from the Fe and FeMo proteins when subjected to different conditions. Of greatest interest is the FeMo cluster where the nitrogen fixation chemistry occurs. As isolated, this cluster exists as a rhombic $S=^{3}/_{2}$ system with g values as 4.32, 3.64 and 2.00.[164] However, most importantly, these EPR signals associated with the Nitrogenase system yield unpaired electron spins that can be used for techniques such as ESEEM, ENDOR and HYSCORE.

Several of the substrates and inhibitors that bind to the FeMo cluster have been characterized in various states using ENDOR in the Hoffman lab. Of great interest are the natures of the intermediate states in the reaction, as they represent snapshots of the chemistry that is occurring during the reduction of N_2. The first study that we will discuss is an EPR/ENDOR examination of the CO inhibited state. This state is produced under turnover conditions in a CO atmosphere and has two signals that appear depending on the CO pressure. The results of this study showed that one CO molecule bound to the cluster under low CO pressure, while two were bound at high pressures. These results were accomplished by using ^{13}CO.[165, 166] Owing to the strong g anisotropy of the EPR signal, both the isotropic and anisotropic components of the hyperfine interactions were

determined. When the g anisotropy is well resolved, techniques like ENDOR can be conducted as a function of the magnetic flied across the EPR envelope. The resulting ENDOR spectra show single crystal like orientation dependences which can allow both the determination of the anisotropic hyperfine interactions, but also their orientation compared to the g value frame. When the results for the low pressure system were compared to other CO-M bound systems, it was determined that there was likely a single CO molecule bridging two Fe atoms via the ^{13}C atom. When the pressure was increased, two CO molecules were detected that were bound to Fe atoms within the cluster through the ^{13}C atoms in a non-bridging arrangement. They were also able to suggest the likely location of the binding as the “waist” portion of the FeMo cluster.[165]

Studies of inhibited intermediates occurred first owing to their relative ease of preparation. However, true intermediates along the N_2 reaction pathway were more difficult to prepare as they are typically very short-lived. To trap some of these intermediate states, researchers used a clever combination of targeted mutations, rapid freeze quench techniques and isotopic substitutions. By creating several key mutations, supplementing the sample with various intermediate state analogues and freeze quenching the system under turnover conditions, the researchers were able to examine their interaction with the FeMo cluster. Several EPR methods were combined to give insight into the intermediate states and the general reaction pathway. The researchers used a double mutant of the enzyme which allows the system to be trapped in an intermediate state.[167] They then used three different substrates ($^{15}N_2H_4$, $^{15}N_2H_2$ and $^{15}N{=}N{-}CH_3$ (MD and characterized the trapped intermediate with each of these substrates using ^{15}N ReMims ENDOR (Figure 16). The results showed that each of these substrates shared a common trapped intermediate state. This was taken as evidence that each of these intermediates plugs into the common reaction pathway from N_2 to 2 NH_3. These results also suggest that the most likely reaction pathway for nitrogen fixation occurs in a manner where protons are added alternately to each nitrogen from N_2 as opposed to the so called “distal” mechanism where three protons are added to the first nitrogen releasing one molecule of NH_3 followed by the hydrolysis of the second nitrogen.

Metal Replacement

While there are large numbers of EPR active metal-based systems within nature, there are still many that are EPR silent due to the identity of the metal. Of particular importance in nature are Mg and Zn. Many systems require Zn for function. Since Zn(II) is a d^{10} system, there are no unpaired electrons to study using EPR. However, many of these systems can be functionally substituted with Co(II), giving an EPR-active probe within the system. One important biological system that has been studied in this manner is the metallo-β-lactamase family of enzymes.[168, 169] These enzymes are a primary target for antibiotic drug design and have been well characterized by the replacement of Zn(II) with Co(II) for EPR studies. Another system where metal replacement has allowed for extensive EPR studies is the interaction of nucleic acids with Mg^{2+}. While Mg^{2+} is EPR silent, it can be functionally replaced with Mn^{2+}, giving a spectroscopic probe that has been extensively utilized to help understand the role of the counter ion in the structure and function of nucleic acids.[170]

Conclusion

In this review, several key examples were provided to show biological researchers that EPR spectroscopy is a powerful biophysical technique that can be used to answer important biological questions. EPR spectroscopy can be used to complement existing structural biology methods or provide pertinent information when traditional techniques cannot be used.

Acknowledgments

Researchers of this work were supported with funds provided by the National Institutes of Health (R01 GM080542 and R01 GM108026) and the National Science Foundation (CHE-1011909 and CHE-1305664).

References

1. Klug CS, Feix JB. Methods and Applications of Site-Directed Spin Labeling EPR Spectroscopy. Methods Cell Biol. 2008; 84:617–658. [PubMed: 17964945]
2. Fanucci GE, Cafiso DS. Recent advances and applications of site-directed spin labeling. Curr Opinion Struct Biol. 2006; 16:644–653.
3. Weil, JA.; Bolton, JR. Electron paramagnetic resonance : Elementary Theory and Practical Applications. Wiley-Interscience; Hoboken, N.J: 2007.
4. Feher G. Observation of Nuclear Magnetic Resonances via the Electron Spin Resonance Line. Phys Rev. 1956; 103:834–835.
5. Mims WB. Pulsed Endor Experiments. Proceedings of the Royal Society of London Series A Mathematical and Physical Sciences. 1965; 283:452–457.
6. Davies ER. A new pulse endor technique. Physics Letters A. 1974; 47:1–2.
7. Schweiger, A.; Jeschke, G. Principles of Pulse Electron Paramagnetic Resonance. Oxford University Press; New York: 2001.
8. Rowan LG, Hahn EL, Mims WB. Electron-Spin-Echo Envelope Modulation. Phys Rev. 1965; 137:A61–A71.
9. Mims WB. Envelope Modulation in Spin-Echo Experiments. Phys Rev B. 1972; 5:2409–2019.
10. Dikanov, SA.; Tsvetkov, Y. Electron Spin Echo Envelope Modulation (ESEEM) Spectroscopy. CRC Press; 1992.
11. Höfer P, Grupp A, Nebenführ H, Mehring M. Hyperfine sublevel correlation (HYSCORE) spectroscopy: a 2D ESR investigation of the squaric acid radical. Chem Phys Lett. 1986; 132:279–282.
12. Pannier M, Veit S, Godt A, Jeschke G, Spiess HW. Dead-time free measurement of dipole-dipole interactions between electron spins. J Magn Reson. 2000; 142:331–340. [PubMed: 10648151]
13. Jeschke G, Polyhach Y. Distance measurements on spin-labelled biomacromolecules by pulsed electron paramagnetic resonance. Physical Chemistry Chemical Physics. 2007; 9:1895–1910. [PubMed: 17431518]
14. Klare JP. Site-Directed Spin Labelingand Electron Paramagnetic Resonance (EPR) Spectroscopy: A Versatile Tool to Study Protein-Protein Interaction. 2012 In Tech.
15. Hubbell WL, Gross A, Langen R, Lietzow MA. Recent advances in site-directed spin labeling of proteins. Curr Opinion Struct Biol. 1998; 8:649–656.
16. Berliner LJ. From spin-labeled proteins to in vivo EPR applications. Eur Biophys J. 2010; 39:579–588. [PubMed: 19763562]
17. Klug CS, Feix JB. SDSL: A survey of biological applications. Biol Magn Reson. 2004; 24:269–308.
18. Drescher M. EPR in protein science : intrinsically disordered proteins. Topics curent chem. 2012; 321:91–119.
19. Feix, JB.; Klug, CS. Biological Magnetic Resonance. Springer; US: 2002. Site-Directed Spin Labeling of Membrane Proteins and Peptide-Membrane Interactions; p. 251-281.
20. Wuthrich K. NMR studies of structure and function of biological macromolecules (Nobel Lecture). J Biomol NMR. 2003; 27:13–39. [PubMed: 15143746]
21. Acharya KR, Lloyd MD. The advantages and limitations of protein crystal structures. Trends Pharmacol Sci. 2005; 26:10–14. [PubMed: 15629199]
22. Schiemann O, Prisner TF. Long-range distance determinations in biomacromolecules by EPR spectroscopy. Quarterly Rev Biophys. 2007; 40:1–53.
23. Torres J, Stevens TJ, Samso M. Membrane proteins: the ‘Wild West’ of structural biology. Trends Biochem Sci. 2003; 28:137–144. [PubMed: 12633993]

24. Columbus L, Hubbell WL. A new spin on protein dynamics. Trends Biochem Sci. 2002; 27:288–295. [PubMed: 12069788]
25. Qin PZ, Dieckmann T. Application of NMR and EPR methods to the study of RNA. Curr Opinion Struct Biol. 2004; 14:350–359.
26. Speicher DW. Characterization of protein primary structure. Dev Biol Stan. 1998; 96:27–28.
27. Klare JP, Steinhoff HJ. Spin labeling EPR. Photosynthesis Research. 2009; 102:377–390. [PubMed: 19728138]
28. Hubbell WL, McHaourab HS, Altenbach C, Lietzow MA. Watching proteins move using site-directed spin labeling. Structure. 1996; 4:779–783. [PubMed: 8805569]
29. Janez S, Tilen K, Zoran A, Bogdan F, David S, A HM. Spin Label EPR-Based Characterization of Biosystem Complexity. J Chem Inf Model. 2005; 45:394–406. [PubMed: 15807505]
30. Hustedt EJ, Beth AH. Nitroxide spin-spin interactions: Applications to protein structure and dynamics. Annu Rev Biophys Biomol Struct. 1999; 28:129–153. [PubMed: 10410798]
31. Hustedt EJ, Smirnov AI, Laub CF, Cobb CE, Beth AH. Molecular distances from dipolar coupled spin-labels: The global analysis of multifrequency continuous wave electron paramagnetic resonance data. Biophys J. 1997; 72:1861–1877. [PubMed: 9083690]
32. Liu KJ, Gast P, Moussavi M, Norby SW, Vahidi N, Walczak T, Wu M, Swartz HM. Lithium Phthalocyanine - A Probe for Electron-Paramagnetic-Resonance Oximetry in Viable Biological-Systems. Proc Natl Acad Sci U S A. 1993; 90:5438–5442. [PubMed: 8390665]
33. Bordignon E, Steinhoff HJ. Membrane protein structure and dynamics studied by site-directed spin-labeling ESR. ESR Spectroscopy in Membrane Biophysics. 2007; 27:129–164.
34. Jeschke G, Bender A, Schweikardt T, Panek G, Decker H, Paulsen H. Localization of the N-terminal domain in light-harvesting chlorophyll a/b protein by EPR measurements. J Biol Chem. 2005; 280:18623–18630. [PubMed: 15755729]
35. Mchaourab, HS.; Perozo, E. Determination of Protein Folds and Conformational Dynamics Using Spin-Labeling EPR Spectroscopy. In: Berliner, L.; Eaton, G.; Eaton, S., editors. Biological Magnetic Resonance. Springer; US: 2002. p. 185-247.
36. Perozo E, Cortes DM, Cuello LG. Three-dimensional architecture and gating mechanism of a K+ channel studied by EPR spectroscopy. Nat Struct Biol. 1998; 5:459–469. [PubMed: 9628484]
37. Vasquez V, Sotomayor M, Cortes DM, Roux B, Schulten K, Perozo E. Three-dimensional architecture of membrane-embedded MscS in the closed conformation. J Mol Biol. 2008; 378:55–70. [PubMed: 18343404]
38. Stone TJ, Buckman T, Nordio PL, McConnel Hm. Spin-Labeled Biomolecules. Proc Natl Acad Sci U S A. 1965; 54:1010–1017. [PubMed: 5219813]
39. Cornish VW, Benson DR, Altenbach CA, Hideg K, Hubbell WL, Schultz PG. Site-specific incorporation of biophysical probes into proteins. Proc Natl Acad Sci U S A. 1994; 91:2910–2914. [PubMed: 8159678]
40. Steinhoff HJ. Multi-frequency EPR spectroscopy studies of the structure and conformational changes of site-directed spin labelled membrane proteins. Supramolecular Structure and Function. 2004; 8:157–177.
41. Stoll S, Schweiger A. Easyspin: simulating cw ESR spectra. Biol Magn Reson. 2007; 27:299–321.
42. Columbus L, Kalai T, Jeko J, Hideg K, Hubbell WL. Molecular motion of spin labeled side chains in alpha-helices: Analysis by variation of side chain structure. Biochemistry. 2001; 40:3828–3846. [PubMed: 11300763]
43. Lietzow MA, Hubbell WL. Motion of spin label side chains in cellular retinol-binding protein: Correlation with structure and nearest-neighbor interactions in an antiparallel beta-sheet. Biochemistry. 2004; 43:3137–3151. [PubMed: 15023065]
44. Cuello LG, Cortes DM, Perozo E. Molecular architecture of the KvAP voltage-dependent K+ channel in a lipid bilayer. Science. 2004; 306:491–495. [PubMed: 15486302]
45. Budil DE, Lee S, Saxena S, Freed JH. Nonlinear-Least-Squares Analysis of Slow-Motion EPR Spectra in One and Two Dimensions Using a Modified Levenberg–Marquardt Algorithm. J Magn Reson series A. 1996; 120:155–189.

46. Feldmann EA, Ni S, Sahu ID, Mishler CH, Risser DD, Murakami JL, Tom SK, McCarrick RM, Lorigan GA, Tolbert BS, Callahan SM, Kennedy MA. Evidence for Direct Binding between HetR from Anabaena sp PCC 7120 and PatS-5. Biochemistry. 2011; 50:9212–9224. [PubMed: 21942265]
47. Mokdad A, Herrick DZ, Kahn AK, Andrews E, Kim M, Cafiso DS. Ligand-Induced Structural Changes in the Escherichia coli Ferric Citrate Transporter Reveal Modes for Regulating Protein-Protein Interactions. J Mol Biol. 2012; 423:818–830. [PubMed: 22982293]
48. Ferguson AD, Chakraborty R, Smith BS, Esser L, van der Helm D, Deisenhofer J. Structural basis of gating by the outer membrane transporter FecA. Science. 2002; 295:1715–1719. [PubMed: 11872840]
49. Ferguson AD, Amezcua CA, Halabi NM, Chelliah Y, Rosen MK, Ranganathan R, Deisenhofer J. Signal transduction pathway of TonB-dependent transporters. Proc Natl Acad Sci U S A. 2007; 104:513–518. [PubMed: 17197416]
50. Humphrey W, Dalke A, Schulten K. VMD: Visual molecular dynamics. J Mol Graph. 1996; 14:33–38. [PubMed: 8744570]
51. Hess JF, Budamagunta MS, Aziz A, FitzGerald PG, Voss JC. Electron paramagnetic resonance analysis of the vimentin tail domain reveals points of order in a largely disordered region and conformational adaptation upon filament assembly. Protein Science. 2013; 22:47–55. [PubMed: 23109052]
52. Aziz A, Hess JF, Budamagunta MS, Voss JC, FitzGerald PG. Site-directed Spin Labeling and Electron Paramagnetic Resonance Determination of Vimentin Head Domain Structure. J Biol Chem. 2010; 285:15278–15285. [PubMed: 20231271]
53. Fajer, PG. Electron Spin Resonance Labeling in Peptide and Protein Analysis. In: Meyers, RA., editor. Encyclopedia of Analytical Chemistry. John Wiley & Sons Ltd; New York: 2000. p. 5725-5761.
54. Altenbach C, Greenhalgh DA, Khorana HG, Hubbell WL. A Collision Gradient Method to Determine the Immersion Depth of Nitroxides in Lipid Bilayers: Application to Spin-Labeled Mutants of Bacteriorhodopsin. Proc Natl Acad Sci U S A. 1994; 91:1667–1671. [PubMed: 8127863]
55. Dong JH, Yang GY, McHaourab HS. Structural basis of energy transduction in the transport cycle of MsbA. Science. 2005; 308:1023–1028. [PubMed: 15890883]
56. Malmberg NJ, Falke JJ. Use of EPR power saturation toanalyze the membrane-docking geometries of peripheral proteins: A applications to C2 domains. Annu Rev Biophys Biomol Struct. 2005; 34:71–90. [PubMed: 15869384]
57. Yu YG, Thorgeirsson TE, Shin YK. Topology of an amphiphilic mitochondrial signal sequence in the membrane-inserted state: A spin-labeling study. Biochemistry. 1994; 33:14221–14226. [PubMed: 7947833]
58. Klug CS, Su WY, Feix JB. Mapping of the residues involved in a proposed beta-strand located in the ferric enterobactin receptor FepA using site-directed spin-labeling. Biochemistry. 1997; 36:13027–13033. [PubMed: 9335564]
59. Coey AT, Sahu ID, Gunasekera TS, Troxel KR, Hawn JM, Swartz MS, Wickenheiser MR, Reid Rj, Welch RC, Vanoye CG, Kang C, Sanders CR, Lorigan GA. Reconstitution of KCNE1 into Lipid Bilayers: Comparing the Structural, Dynamic, and Activity Differences in Micelle and Vesicle Environments. Biochemistry. 2011; 50:10851–10859. [PubMed: 22085289]
60. Kang C, Tian C, Sonnichsen FD, Smith JA, Meiler J, George ALJ, Vanoye CG, Kim HJ, Sanders CR. Structure of KCNE1 and Implications for How It Modulates the KCNQ1Potassium Channel. Biochemistry. 2008; 47:7999–8006. [PubMed: 18611041]
61. Voss J, He MM, Hubbell WL, Kaback HR. Site-directed spin labeling demonstrates that transmembrane domain XII in the lactose permease of Escherichia coli is an alpha-helix. Biochemistry. 1996; 35:12915–12918. [PubMed: 8841136]
62. Guan L, Mirza O, Verner G, Iwata S, Kaback HR. Structural determination of wild-type lactose permease. Proc Natl Acad Sci U S A. 2007; 104:15294–15298. [PubMed: 17881559]

63. Inbaraj JJ, Cardon TB, Laryukhin M, Grosser SM, Lorigan GA. Determining the topology of integral membrane peptides using EPR spectroscopy. J Am Chem Soc. 2006; 128:9549–9554. [PubMed: 16848493]
64. Ghimire H, Hustedt EJ, Sahu ID, Inbaraj JJ, McCarrick R, Mayo DJ, Benedikt MR, Lee RT, Grosser SM, Lorigan GA. Distance Measurements on a Dual-Labeled TOAC AChR M2δ Peptide in Mechanically Aligned DMPC Bilayers via Dipolar Broadening CW-EPR Spectroscopy. J Phys Chem B. 2012; 116:3866–3873. [PubMed: 22379959]
65. Liang Z, Freed JH. An Assessment of the Applicability of Multifrequency ESR to Study the Complex Dynamics of Biomolecules. J Phys Chem B. 1999; 103:6384–6396.
66. Zhang ZW, Fleissner MR, Tipikin DS, Liang ZC, Moscicki JK, Earle KA, Hubbell WL, Freed JH. Multifrequency Electron Spin Resonance Study of the Dynamics of Spin Labeled T4 Lysozyme. J Phys Chem B. 2010; 114:5503–5521. [PubMed: 20361789]
67. Earle, KA.; Smirnov, AI. Biological Magnetic Resonance. Kluwer Academic/Plenum Publication; 2004. High Field ESR: Applications to Protein Structure and Dynamics; p. 95-141.
68. Savitsky A, Mobius K. High-field EPR. Photosynthesis Research. 2009; 102:311–333. [PubMed: 19468856]
69. Borbat PP, Costa-Filho AJ, Earle KA, Moscicki JK, Freed JH. Electron spin resonance in studies of membranes and proteins. Science. 2001; 291:266–269. [PubMed: 11253218]
70. Mobius K, Savitsky A. High-Field EPR Spectroscopy on Proteins and their Model Systems: Characterization of Transient Paramagnetic States. 2008
71. Mobius K, Savitsky A, Schnegg A, Plato M, Fuchs M. High-field EPR spectroscopy applied to biological systems: characterization of molecular switches for electron and ion transfer. Phys Chem Chem Phys. 2005; 7:19–42. [PubMed: 19785170]
72. Nesmelov YE, Agafonov RV, Burr AR, Weber RT, Thomas DD. Structure and dynamics of the force-generating domain of myosin probed by multifrequency electron paramagnetic resonance. Biophys J. 2008; 95:247–256. [PubMed: 18339764]
73. Bauer CB, Holden HM, Thoden JB, Smith R, Rayment I. X-ray structures of the apo and MgATP-bound states of Dictyostelium discoideum myosin motor domain. J Biol Chem. 2000; 275:38494–38499. [PubMed: 10954715]
74. Harrington WF, Rodgers ME. MYOSIN. Ann Rev Biochem. 1984; 53:35–73. [PubMed: 6383197]
75. McCracken, J. Encyclopedia of Inorganic and Bioinorganic Chemistry. John Wiley & Sons, Ltd.; 2011. Electron Spin Echo Envelope Modulation (ESEEM) Spectroscopy.
76. Cieslak JA, Focia PJ, Gross A. Electron Spin-Echo Envelope Modulation (ESEEM) Reveals Water and Phosphate Interactions with the KcsA Potassium Channel. Biochemistry. 2010; 49:1486–1494. [PubMed: 20092291]
77. Zhou A, Abu-Baker S, Sahu ID, Liu L, McCarrick RM, Dabney-Smith C, Lorigan GA. Determining α-Helical and β-Sheet Secondary Structures via Pulsed Electron Spin Resonance Spectroscopy. Biochemistry. 2012; 51:7417–7419. [PubMed: 22966895]
78. Volkov A, Dockter C, Polyhach Y, Paulsen H, Jeschke G. Site-Specific Information on Membrane Protein Folding by Electron Spin Echo Envelope Modulation Spectroscopy. J Phys Chem Lett. 2010; 1:663–667.
79. Dzuba SA, Raap J. Spin-Echo Electron Paramagnetic Resonance (EPR) Spectroscopy of a Pore-Forming (Lipo)Peptaibol in Model and Bacterial Membranes. Chemistry & biodiversity. 2013; 10:864–875. [PubMed: 23681730]
80. Sun L, Hernandez-Guzman J, Warncke K. OPTESIM, a versatile toolbox for numerical simulation of electron spin echo envelope modulation (ESEEM) that features hybrid optimization and statistical assessment of parameters. J Magn Reson. 2009; 200:21–28. [PubMed: 19553148]
81. Liu L, Sahu ID, Mayo DJ, McCarrick RM, Troxel K, Zhou A, Shockley E, Lorigan GA. Enhancement of Electron Spin Echo Envelope Modulation Spectroscopic Methods to Investigate the Secondary Structure of Membrane Proteins. J Phys Chem B. 2012; 116:11041–11045. [PubMed: 22908896]
82. Mayo D, Zhou A, Sahu I, McCarrick R, Walton P, Ring A, Troxel K, Coey A, Hawn J, Emwas AH, Lorigan GA. Probing the structure of membrane proteins with electron spin echo envelope modulation spectroscopy. Protein Science. 2011; 20:1100–1104. [PubMed: 21563228]

83. Chiang YW, Zheng TY, Kao CJ, Horng JC. Determination of Interspin Distance Distributions by cw-ESR Is a Single Linear Inverse Problem. Biophys J. 2009; 97:930–936. [PubMed: 19651052]
84. Kittell AW, Hustedt EJ, Hyde JS. Inter-spin distance determination using L-band (1-2 GHz) non-adiabatic rapid sweep electron paramagnetic resonance (NARS EPR). J Magn Reson. 2012; 221:51–56. [PubMed: 22750251]
85. Rabenstein MD, Shin YK. Determination of the distance between 2 spin labels attached to a macromolecule. Proc Natl Acad Sci U S A. 1995; 92:8239–8243. [PubMed: 7667275]
86. Altenbach C, Oh KJ, Trabanino RJ, Hideg K, Hubbell WL. Estimation of inter-residue distances in spin labeled proteins at physiological temperatures: Experimental strategies and practical limitations. Biochemistry. 2001; 40:15471–15482. [PubMed: 11747422]
87. McHaourab HS, Oh KJ, Fang CJ, Hubbell WL. Conformation of T4 lysozyme in solution. Hinge-bending motion and the substrate-induced conformational transition studied by site-directed spin labeling. Biochemistry. 1997; 36:307–316. [PubMed: 9003182]
88. Hanelt I, Wunnicke D, Muller-Trimbusch M, Vor der Bruggen M, Kraus I, Bakker EP, Steinhoff HJ. Membrane Region M-2C2 in Subunit KtrB of the K+ Uptake System KtrAB from Vibrio alginolyticus Forms a Flexible Gate Controlling K+ Flux: An Electron Paramagnetic Resonance Study. J Biol Chem. 2010; 285:28210–28219. [PubMed: 20573964]
89. Borbat PP, McHaourab HS, Freed JH. Protein structure determination using long-distance constraints from double-quantum coherence ESR: Study of T4 lysozyme. J Am Chem Soc. 2002; 124:5304–5314. [PubMed: 11996571]
90. Schiemann O, Piton N, Mu YG, Stock G, Engels JW, Prisner TF. A PELDOR-based nanometer distance ruler for oligonucleotides. J Am Chem Soc. 2004; 126:5722–5729. [PubMed: 15125665]
91. Milov AD, Tsvetkov YD, Formaggio F, Crisma M, Toniolo C, Raap J. Self-assembling properties of membrane-modifying peptides studied by PELDOR and CW-ESR spectroscopies. J Am Chem Soc. 2000; 122:3843–3848.
92. Hilger D, Jung H, Padan E, Wegener C, Vogel KP, Steinhoff HJ, Jeschke G. Assessing oligomerization of membrane proteins by four-pulse DEER: pH-dependent dimerization of NhaA Na+/H+ antiporter of E-coli. Biophys J. 2005; 89:1328–1338. [PubMed: 15894644]
93. Jeschke G. DEER Distance Measurements on Proteins. Annu Rev Phys Chem. 2012:419–446. [PubMed: 22404592]
94. Banham JE, Timmel CR, Abbott RJM, Lea SM, Jeschke G. The characterization of weak protein-protein interactions: evidence from DEER for the trimerization of a von Willebrand Factor A domain in solution. Angew Chem Int Ed. 2006; 45:1058–1061.
95. Reginsson GW, Hunter RI, Cruickshank PAS, Bolton DR, Sigurdsson ST, Smith GM, Schiemann O. W-band PELDOR with 1 kW microwave power: Molecular geometry, flexibility and exchange coupling. J Magn Reson. 2012; 216:175–182. [PubMed: 22386646]
96. Prisner T, Rohrer M, MacMillan F. Pulsed EPR spectroscopy: Biological applications. Annu Rev Phys Chem. 2001; 52:279–313. [PubMed: 11326067]
97. McHaourab HS, Steed PR, Kazmier K. Toward the fourth dimension of membrane protein structure: insight into dynamics from spin-labeling EPR spectroscopy. Structure. 2011; 19:1549–1561. [PubMed: 22078555]
98. Ghimire H, McCarrick RM, Budil DE, Lorigan GA. Significantly Improved Sensitivity of Q-Band PELDOR/DEER Experiments Relative to X-Band Is Observed in Measuring the Intercoil Distance of a Leucine Zipper Motif Peptide (GCN4-LZ). Biochemistry. 2009; 48:5782–5784. [PubMed: 19476379]
99. Polyhach Y, Bordignon E, Tschaggelar R, Gandra S, Godt A, Jeschke G. High sensitivity and versatility of the DEER experiment on nitroxide radical pairs at Q-band frequencies. Phys Chem Chem Phys. 2012; 14:10762–10773. [PubMed: 22751953]
100. Zou P, McHaourab HS. Increased Sensitivity and Extended Range of Distance Measurements in Spin-Labeled Membrane Proteins: Q-Band Double Electron-Electron Resonance and Nanoscale Bilayers. Biophys J. 2010; 98:L18–L20. [PubMed: 20303847]
101. Höfer P, Heilig R, Schmalbein D. The superQ-FT accessory for pulsed EPR, ENDOR and ELDOR at 34 GHz. Bruker Spin Report. 2003:37–43.

102. Fleissner MR, Bridges MD, Brooks EK, Cascio D, Kálai T, Hideg K, Hubbell WL. Structure and dynamics of a conformationally constrained nitroxide side chain and applications in EPR spectroscopy. Proc Natl Acad Sci U S A. 2012; 108:16241–16246. [PubMed: 21911399]
103. Jao CC, Hegde BG, Chen J, Haworth IS, Langen R. Structure of membrane-bound alpha-synuclein from site-directed spin labeling and computational refinement. Proc Natl Acad Sci U S A. 2008; 105:19666–19671. [PubMed: 19066219]
104. Hirst SJ, Alexander N, McHaourab HS, Meiler J. RosettaEPR: an integrated tool for protein structure determination from sparse EPR data. J Struct Biol. 2011; 173:506–514. [PubMed: 21029778]
105. Barrett PJ, Song Y, Van Horn WD, Hustedt EJ, Schafer JM, Hadziselimovic A, Beel AJ, Sanders CR. The Amyloid Precursor Protein Has a Flexible Transmembrane Domain and Binds Cholesterol. Science. 2012; 336:1168–1171. [PubMed: 22654059]
106. Dixit M, Kim S, Matthews GF, Erreger K, Galli A, Cobb CE, Hustedt EJ, Beth AH. Structural Arrangement of the Intracellular Ca2+ Binding Domains of the Cardiac Na+/Ca2+ Exchanger (NCX1.1) Effects of Ca2+ Binding. J Biol Chem. 2013; 288:4194–4207. [PubMed: 23233681]
107. Hilger D, Polyhach Y, Jung H, Jeschke G. Backbone Structure of Transmembrane Domain IX of the Na+/Proline Transporter PutP of Escherichia coli. Biophys J. 2009; 96:217–225. [PubMed: 19134477]
108. Raba M, Baumgartner T, Hilger D, Klempahn K, Haertel T, Jung K, Jung H. Function of transmembrane domain IX in the Na(+)/proline transporter PutP. J of Mol Biol. 2008; 382:884–893. [PubMed: 18692508]
109. Jung H, Rubenhagen R, Tebbe S, Leifker K, Tholema N, Quick M, Schmid R. Topology of the Na+/Proline transporter of Escherichia coli. J Biol Chem. 1998; 273:26400–26407. [PubMed: 9756872]
110. Wegener C, Tebbe S, Steinhoff HJ, Jung HR. Spin labeling analysis of structure and dynamics of the Na+/proline transporter of Escherichia coli. Biochemistry. 2000; 39:4831–4837. [PubMed: 10769140]
111. Endeward B, Butterwick JA, MacKinnon R, Prisner TF. Pulsed Electron-Electron Double-Resonance Determination of Spin-Label Distances and Orientations on the Tetrameric Potassium Ion Channel KcsA. J Am Chem Soc. 2009; 131:15246–15250. [PubMed: 19919160]
112. Reichmann D, Rahat O, Cohen M, Neuvirth H, Schreiber G. The molecular architecture of protein-protein binding sites. Curr Opinion Struct Biol. 2007; 17:67–76.
113. Sarewicz M, Szytula S, Dutka M, Osyczka A, Froncisz W. Estimation of binding parameters for the protein-protein interaction using a site-directed spin labeling and EPR spectroscopy. Eur Biophys J Biophys Lett. 2008; 37:483–493.
114. Kim S, Brandon S, Zhou Z, Cobb CE, Edwards SJ, Moth CW, Parry CS, Smith JA, Lybrand TP, Hustedt EJ, Beth AH. Determination of Structural Models of the Complex between the Cytoplasmic Domain of Erythrocyte Band 3 and Ankyrin-R Repeats 13-24. J Biol Chem. 2011; 286:20746–20757. [PubMed: 21493712]
115. Braun P, Naegele B, Wittmann V, Drescher M. Mechanism of Multivalent Carbohydrate-Protein Interactions Studied by EPR Spectroscopy. Angew Chem, Int Ed. 2011; 50:8428–8431.
116. Herget M, Baldauf C, Scholz C, Parcej D, Wiesmuller KH, Tampe R, Abele R, Bordignon E. Conformation of peptides bound to the transporter associated with antigen processing (TAP). Proc Natl Acad Sci U S A. 2011; 108:1349–1354. [PubMed: 21205905]
117. James ZM, McCaffrey JE, Torgersen KD, Karim CB, Thomas DD. Protein-Protein Interactions in Calcium Transport Regulation Probed by Saturation Transfer Electron Paramagnetic Resonance. Biophysi J. 2012; 103:1370–1378.
118. Stoll, S. High-field EPR of bioorganic radicals. Vol. 22. Royal Society of Chemistry; 2011.
119. Stoll S, Gunn A, Brynda M, Sughrue W, Kohler AC, Ozarowski A, Fisher AJ, Lagarias JC, Britt RD. Structure of the Biliverdin Radical Intermediate in Phycocyanobilin:Ferredoxin Oxidoreductase Identified by High-Field EPR and DFT. J Am Chem Soc. 2009; 131:1986–1995. [PubMed: 19159240]

120. Tu SL, Rockwell NC, Lagarias JC, Fisher AJ. Insight into the radical mechanism of phycocyanobilin-ferredoxin oxidoreductase (PcyA) revealed by X-ray crystallography and biochemical measurements. Biochemistry. 2007; 46:1484–1494. [PubMed: 17279614]

121. Tu SL, Gunn A, Toney MD, Britt RD, Lagarias JC. Biliverdin reduction by cyanobacterial phycocyanobilin : ferredoxin oxidoreductase (PcyA) proceeds via linear tetrapyrrole radical intermediates. J Am Chem Soc. 2004; 126:8682–8693. [PubMed: 15250720]

122. Stubbe, J.; Cotruvo, JA. Ribonucleotide Reductase: Recent Advances. Vol. 4. John Wiley & Sons Ltd.; 2011.

123. Barry BA, Chen J, Keough J, Jenson D, Offenbacher A, Pagba C. Proton-Coupled Electron Transfer and Redox-Active Tyrosines: Structure and Function of the Tyrosyl Radicals in Ribonucleotide Reductase and Photosystem II. J Phys Chem Lett. 2012; 3:543–554. [PubMed: 22662289]

124. Sjoberg BM, Reichard P, Graslund A, Ehrenberg A. Nature of Free-Radical in Ribonucleotide Reductase from Escherichia-Coli. J Biol Chem. 1977; 252:536–541. [PubMed: 188819]

125. Sjoberg BM, Reichard P, Graslund A, Ehrenberg A. Tyrosine Free-Radical in Ribonucleotide Reductase from Escherichia-Coli. J Biol Chem. 1978; 253:6863–6865. [PubMed: 211133]

126. Tomter AB, Zoppellaro G, Schmitzberger F, Andersen NH, Barra AL, Engman H, Nordlund P, Andersson KK. HF-EPR, Raman, UV/VIS Light Spectroscopic, and DFT Studies of the Ribonucleotide Reductase R2 Tyrosyl Radical from Epstein-Barr Virus. Plos One. 2011; 6:e25022. [PubMed: 21980375]

127. Hogbom M, Galander M, Andersson M, Kolberg M, Hofbauer W, Lassmann G, Nordlund P, Lendzian F. Displacement of the tyrosyl radical cofactor in ribonucleotide reductase obtained by single-crystal high-field EPR and 1.4-angstrom x-ray data. Proc Natl Acad Sci U S A. 2003; 100:3209–3214. [PubMed: 12624184]

128. Gerfen GJ, Bellew BF, Un S, Bollinger JM, Stubbe J, Griffin RG, Singel DJ. High-Frequency (139.5 Ghz) EPR Spectroscopy of the Tyrosyl Radical in Escherichia-Coli Ribonucleotide Reductase. J Am Chem Soc. 1993; 115:6420–6421.

129. Lendzian F. Structure and interactions of amino acid radicals in class I ribonucleotide reductase studied by ENDOR and high-field EPR spectroscopy. Biochim Biophys Acta-Bioenergetics. 2005; 1707:67–90.

130. Crofts AR, Holland JT, Victoria D, Kolling DRJ, Dikanov SA, Gilbreth R, Lhee S, Kuras R, Kuras MG. The Q-cycle reviewed: How well does a monomeric mechanism of the bc(1) complex account for the function of a dimeric complex? Biochim Et Biophys Acta-Bioenergetics. 2008; 1777:1001–1019.

131. Styring S, Sjoholm J, Mamedov F. Two tyrosines that changed the world: Interfacing the oxidizing power of photochemistry to water splitting in photosystem II. Biochim Et Biophys Acta-Bioenergetics. 2012; 1817:76–87.

132. McCarrick, MR.; Britt, RD. Current Models and Mechanism of Water Splitting: Photosynthetic Protein Complexes. Wiley-VCH Verlag GmbH & Co. KGaA; 2008.

133. Umena Y, Kawakami K, Shen JR, Kamiya N. Crystal structure of oxygen-evolving photosystem II at a resolution of 1.9 angstrom. Nature. 2011; 473:55–U65. [PubMed: 21499260]

134. Dismukes GC, Siderer Y. EPR Spectroscopic observations of a Manganese center associated with Water Oxidation in Spinach-Chloroplasts. Febs Lett. 1980; 121:78–80.

135. Dismukes GC, Siderer Y. Intermediates of a Polynuclear Manganese center involved in Photosynthetic Oxidation of Water. Proc Natl Acad Sci U S A. 1981; 78:274–278. [PubMed: 16592949]

136. Zimmermann JL, Rutherford AW. Electron paramagnetic resonance properties of the S2 state of the oxygen-evolving complex of photosystem II. Biochemistry. 1986; 25:4609–4615.

137. Zimmermann JL, Rutherford AW. Electron-Paramagnetic-Resonance studies of the oxygen-evolving Enzyme of Photosystem-II. Biochim Et Biophys Acta. 1984; 767:160–167.

138. Casey JL, Sauer K. Electron-Paramagnetic-Resonance detection of a Cryogenically Photogenerated Intermediate in Photosynthetic oxygen Evolution. Biochim Et Biophys Acta. 1984; 767:21–28.

139. Haddy A, Lakshmi KV, Brudvig GW, Frank HA. Q-band EPR of the S-2 state of Photosystem II confirms an S=5/2 origin of the X-band g=4.1 signal. Biophys J. 2004; 87:2885–2896. [PubMed: 15454478]
140. Kim DH, Britt RD, Klein MP, Sauer K. The Manganese site of the Photosynthetic oxygen-Evolving Complex probed by EPR Spectroscopy of oriented Photosystem-II Membranes - the g = 4 And g = 2 Multiline Signals. Biochemistry. 1992; 31:541–547. [PubMed: 1310041]
141. Pantazis DA, Ames W, Cox N, Lubitz W, Neese F. Two Interconvertible Structures that Explain the Spectroscopic Properties of the Oxygen-Evolving Complex of Photosystem II in the S2 State. Angew Chem, Int Ed. 2012; 51:9935–9940.
142. Messinger J, Nugent JHA, Evans MCW. Detection of an EPR multiline signal for the S-0 state in photosystem II. Biochemistry. 1997; 36:11055–11060. [PubMed: 9333322]
143. Messinger J, Robblee JH, Yu WO, Sauer K, Yachandra VK, Klein MP. The S_0State of the Oxygen-Evolving Complex in Photosystem II Is Paramagnetic:뷰 Detection of an EPR Multiline Signal. J Am Chem Soc. 1997; 119:11349–11350.
144. Dexheimer SL, Klein MP. Detection of a Paramagnetic Intermediate in the S1-State of the Photosynthetic oxygen-evolving Complex. J Am Chem Soc. 1992; 114:2821–2826.
145. Campbell KA, Peloquin JM, Pham DP, Debus RJ, Britt RD. Parallel polarization EPR detection of an S-1-state “multiline” EPR signal in photosystem II particles from Synechocystis sp. PCC 6803. J Am Chem Soc. 1998; 120:447–448.
146. Peloquin JM, Campbell KA, Randall DW, Evanchik MA, Pecoraro VL, Armstrong WH, Britt RD. Mn-55 ENDOR of the S-2-state multiline EPR signal of photosystem II: Implications on the structure of the tetranuclear Mn cluster. J Am Chem Soc. 2000; 122:10926–10942.
147. Britt RD, Peloquin JM, Campbell KA. Pulsed and parallel-polarization EPR characterization of the photosystem II oxygen-evolving complex. Annu Rev Biophys Biomol Struct. 2000; 29:463–495. [PubMed: 10940256]
148. Hasegawa K, Ono TA, Inoue Y, Kusunoki M. Spin-exchange interactions in the S-2-state manganese tetramer in photosynthetic oxygen-evolving complex deduced from g=2 multiline EPR signal. Chem Phys Lett. 1999; 300:9–19.
149. Zheng M, Dismukes GC. Orbital configuration of the valence electrons, ligand field symmetry, and manganese oxidation states of the photosynthetic water oxidizing complex: Analysis of the S-2 state multiline EPR signals. Inorg Chem. 1996; 35:3307–3319. [PubMed: 11666533]
150. Ahrling KA, Pace RJ. Simulation of the S-2 State Multiline Electron-Paramagnetic-Resonance signal of Photosystem-II - A Multifrequency approach. Biophys J. 1995; 68:2081–2090. [PubMed: 7612851]
151. Zouni A, Witt HT, Kern J, Fromme P, Krauss N, Saenger W, Orth P. Crystal structure of photosystem II from Synechococcus elongatus at 3.8 angstrom resolution. Nature. 2001; 409:739–743. [PubMed: 11217865]
152. Kulik LV, Epel B, Lubitz W, Messinger J. Electronic structure of the Mn4OxCa cluster in the S-0 and S-2 states of the oxygen-evolving complex of photosystem II based on pulse Mn-55-ENDOR and EPR Spectroscopy. J Am Chem Soc. 2007; 129:13421–13435. [PubMed: 17927172]
153. Britt RD, Tang XS, Gilchrist ML, Lorigan GA, Larsen BS, Diner BA. Histidine at the Catalytic site of the Photosynthetic oxygen-evolving Complex. Biochem Soc Trans. 1994; 22:343–347. [PubMed: 7958322]
154. Tang XS, Diner BA, Larsen BS, Gilchrist ML, Lorigan GA, Britt RD. Identification of Histidine at the Catalytic site of the Photosynthetic Oxygen-Evolving Complex. Proc Natl Acad Sci U S A. 1994; 91:704–708. [PubMed: 8290585]
155. Yeagle GJ, Gilchrist ML, McCarrick RM, Britt RD. Multifrequency pulsed electron paramagnetic resonance study of the S-2 state of the photosystem II manganese cluster. Inorg Chem. 2008; 47:1803–1814. [PubMed: 18330971]
156. Yeagle GJ, Gilchrist ML Jr, Walker LM, Debus RJ, Britt RD. Multifrequency electron spin-echo envelope modulation studies of nitrogen ligation to the manganese cluster of photosystem II. Philos Trans Royal Soc B-Biol Sci. 2008; 363:1157–1166.

157. Stich TA, Yeagle GJ, Service RJ, Debus RJ, Britt RD. Ligation of D1-His332 and D1-Asp170 to the Manganese Cluster of Photosystem II from Synechocystis Assessed by Multifrequency Pulse EPR Spectroscopy. Biochemistry. 2011; 50:7390–7404. [PubMed: 21790179]

158. Stull JA, Stich TA, Service RJ, Debus RJ, Mandal SK, Armstrong WH, Britt RD. C-13 ENDOR Reveals That the D1 Polypeptide C-Terminus Is Directly Bound to Mn in the Photosystem II Oxygen Evolving Complex. J Am Chem Soc. 2010; 132:446–447. [PubMed: 20038096]

159. Aznar CP, Britt RD. Simulations of the H-1 electron spin echo-electron nuclear double resonance and H-2 electron spin echo envelope modulation spectra of exchangeable hydrogen nuclei coupled to the S-2-state photosystem II manganese cluster. Phil Trans R Soc Lond B. 2002; 357:1359–1365. [PubMed: 12437874]

160. McConnell IL, Grigoryants VM, Scholes CP, Myers WK, Chen PY, Whittaker JW, Brudvig GW. EPR-ENDOR Characterization of (O-17, H-1, H-2) Water in Manganese Catalase and Its Relevance to the Oxygen-Evolving Complex of Photosystem II. J Am Chem Soc. 2012; 134:1504–1512. [PubMed: 22142421]

161. Hoffman BM, Dean DR, Seefeldt LC. Climbing Nitrogenase: Toward a Mechanism of Enzymatic Nitrogen Fixation. Acc Chem Research. 2009; 42:609–619. [PubMed: 19267458]

162. Seefeldt LC, Hoffman BM, Dean DR. Electron transfer in nitrogenase catalysis. Curr Opinion Chem Biol. 2012; 16:19–25.

163. Spatzal T, Aksoyoglu M, Zhang L, Andrade SLA, Schleicher E, Weber S, Rees DC, Einsle O. Evidence for Interstitial Carbon in Nitrogenase FeMo Cofactor. Science. 2011; 334:940–940. [PubMed: 22096190]

164. Ormejohn WH, Hamilton WD, Shah VK, Tso MYW, Burris RH, Brill WJ, Jones TL. Electron-Paramagnetic Resonance of Nitrogenase and Nitrogenase Components from Clostridium-Pasteurianum W5 and Azotobacter-Vinelandii-OP. Proc Natl Acad Sci U S A. 1972; 69:3142–3145. [PubMed: 4343957]

165. Lee HI, Cameron LM, Hales BJ, Hoffman BM. CO binding to the FeMo cofactor of CO-inhibited nitrogenase: (CO)-C-13 and H-1 Q-band ENDOR investigation. J Am Chem Soc. 1997; 119:10121–10126.

166. Pollock RC, Lee HI, Cameron LM, Derose VJ, Hales BJ, Ormejohnson WH, Hoffman BM. Investigation of CO bound to inhibited forms of Nitrogenase MoFe Protein by C-13 ENDOR. J Am Chem Soc. 1995; 117:8686–8687.

167. Lukoyanov D, Dikanov SA, Yang ZY, Barney BM, Samoilova RI, Narasimhulu KV, Dean DR, Seefeldt LC, Hoffman BM. ENDOR/HYSCORE Studies of the Common Intermediate Trapped during Nitrogenase Reduction of N2H2, CH3N2H, and N2H4 Support an Alternating Reaction Pathway for N-2 Reduction. J Am Chem Soc. 2011; 133:11655–11664. [PubMed: 21744838]

168. Crowder MW, Spencer J, Vila AJ. Metallo-beta-lactamases: Novel weaponry for antibiotic resistance in bacteria. Accou Chem Research. 2006; 39:721–728.

169. Griffin DH, Richmond TK, Sanchez C, Moller AJ, Breece RM, Tierney DL, Bennett B, Crowder MW. Structural and Kinetic Studies on Metallo-beta-lactamase IMP-1. Biochemistry. 2011; 50:9125–9134. [PubMed: 21928807]

170. DeRose VJ. Characterization of nucleic acid-metal ion binding by spectroscopic techniques, Royal Society of Chemistry. 2009

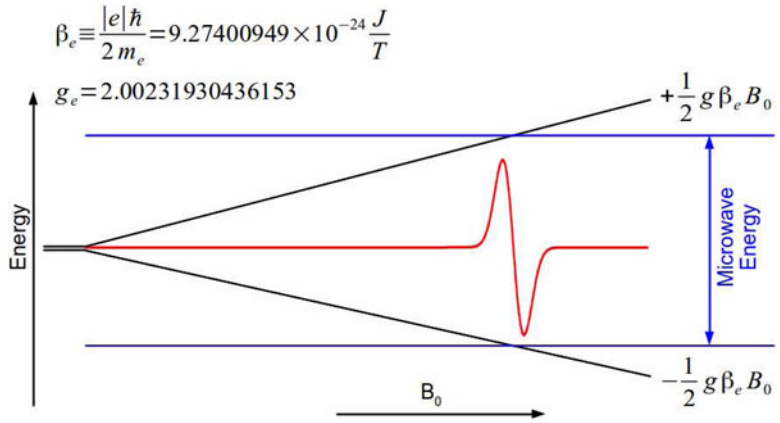

Figure 1.

EPR transitions occur when the energy contained in the microwave photons matches the splitting between two electron spin states. In the simplest system, this splitting as a function of the magnetic field is $g\beta_e B_0$.

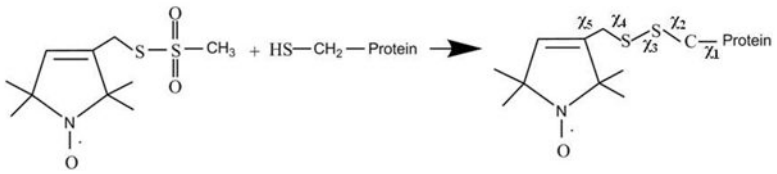

Figure 2.

Structure of MTSL and the resulting side chain produced by reaction with the cysteine residue of the protein. The $\chi 1, \chi 2, \chi 3, \chi 4$ and $\chi 5$ represent the locations of five rotations about the chemical bonds between α-carbon backbone of the protein and the pyrroline ring of the attached MTSL.

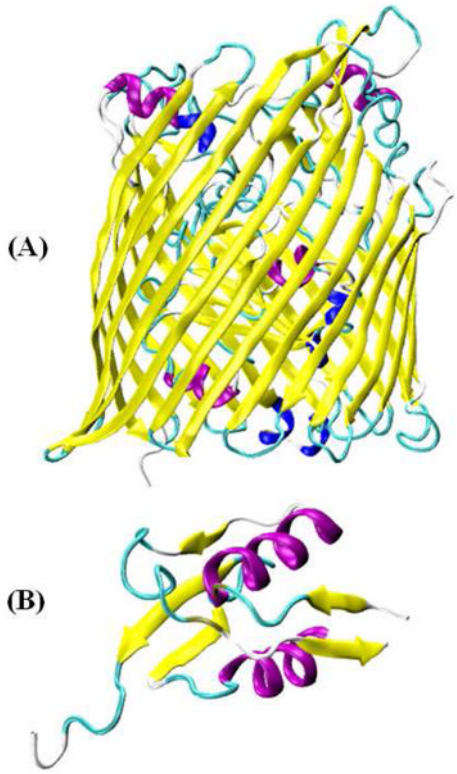

Figure 3.
Representation of TonB-dependent iron transporter: (A) X-ray crystal structure of Escherichia coli ferric citrate transporter FecA (PDB ID: 1KMO)[48] (the N-terminal transcriptional signaling motif was not resolved in FecA), and (B) Solution NMR structure of the N-terminal transcriptional signaling motif of FecA (PDB ID: 1ZZV).[49] Figures were prepared using visual molecular dynamics (VMD) software.[50]

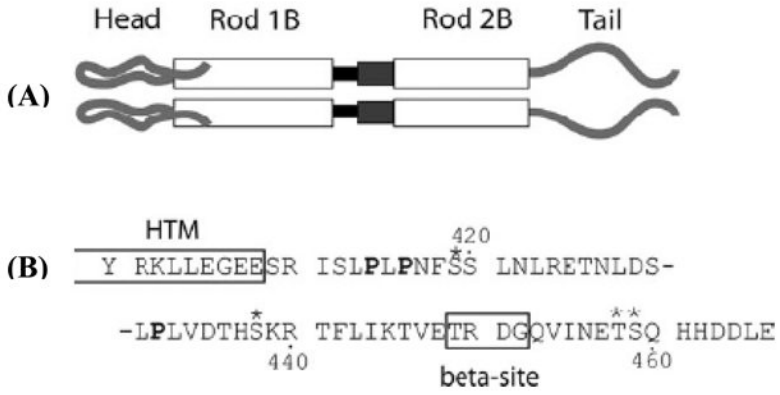

Figure 4.

Schematic of the Vimentin molecular structure. Panel **(A)** shows a representation of the protein domains of Vimentin. At the amino terminus is the head domain, leading into rod domain 1. The black box between rod 1B and rod 2B represents Linker 1-2. The dark gray box between rod 1B and rod 2B represents the parallel helices structure of rod 2A/Linker 2. Panel **(B)** shows the amino acid sequence of the tail domain, beginning with Y^{100}. The HTM and β (beta) sites are boxed and labeled. Prolines are in bold; phosphorylation sites are indicated by asterisks. (Adapted from ref. 51 with permission)

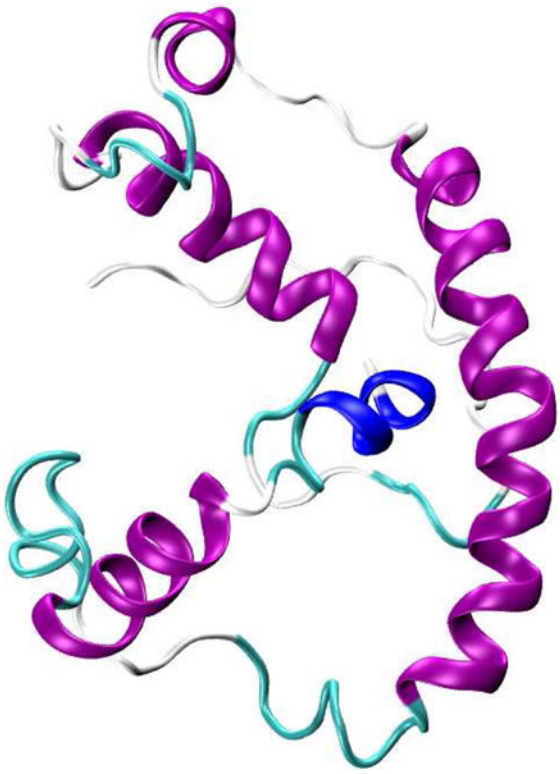

Figure 5.
Representation of the NMR structure of KCNE1 membrane protein in LMPG micelles (PDB ID: 2K21).[60] Figure was prepared using VMD software.[50]

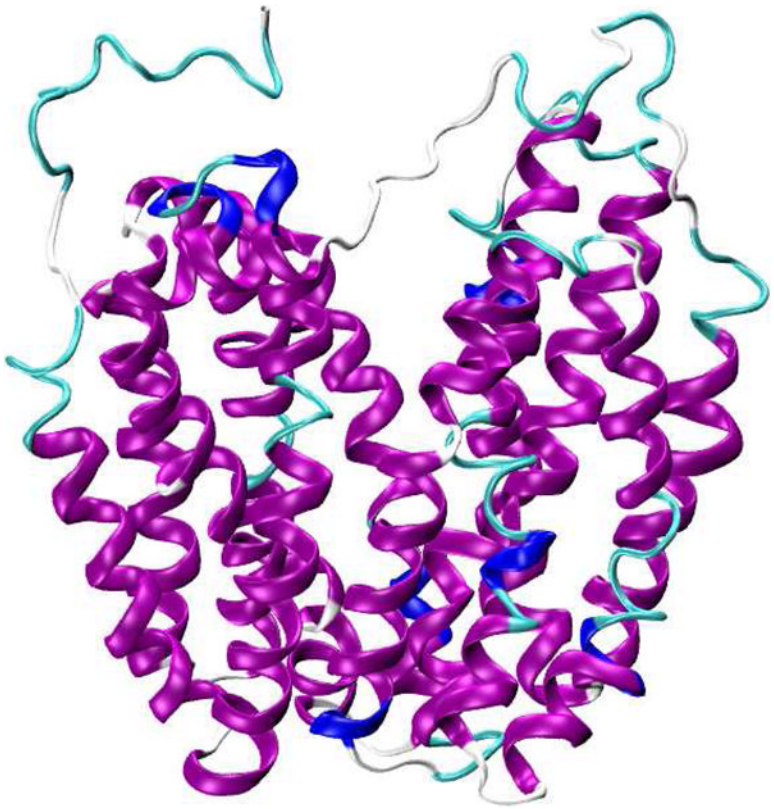

Figure 6.
Representation of X-ray crystal structure of wild-type lactose permease protein (PDB ID: 2V8N).[62] Figure was prepared using VMD software.[50]

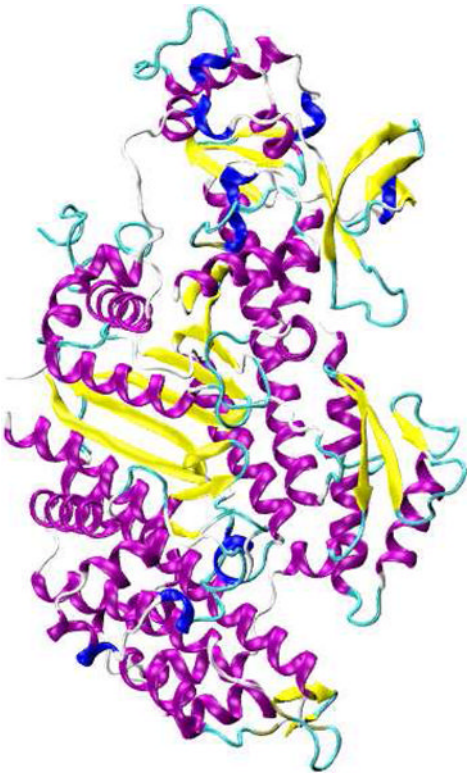

Figure 7.
Representation of X-ray crystal structure of the motor domain of Dictyostelium discoideum myosin II (PDB ID: 1FMV).[73] Figure was prepared using VMD software.[50]

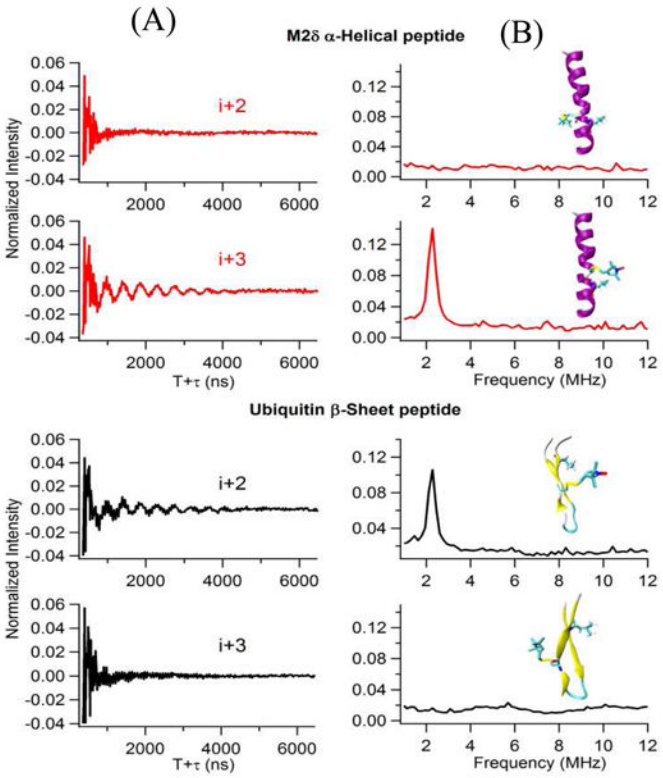

Figure 8.

Three-pulse ESEEM experimental data with a τ=200ns of the *i*+2 and the *i*+3 ^{2}H-labeled Leu for AchR M2δ helical peptide in lipid bilayer and ubiquitin β-sheet peptide in solution. (A) Time domain, (B) Frequency domain. The inset structural pictures show the location of spin labels and ^{2}H-labeled Leu on AchR M2δ helical peptide and ubiquitin β-sheet peptide. (Adapted from ref. 77 with permission)

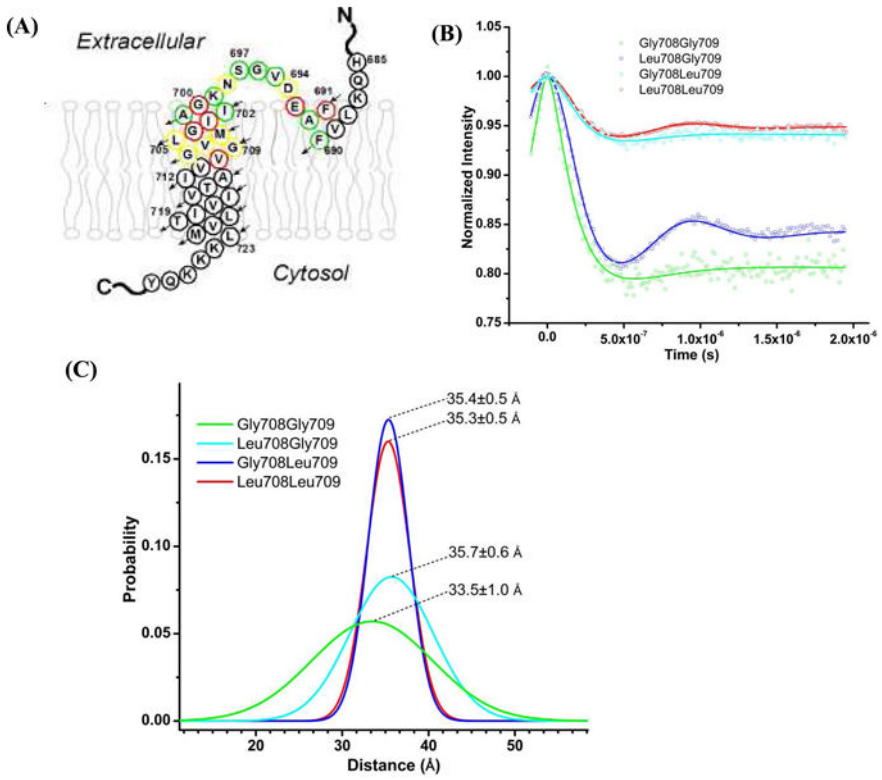

Figure 9.

DEER data used to identify the curvature helicity of the transmembrane region of Amyloid Precursor Protein (C99) in POPC/POPG vesicle system. (A) Topological illustration of C99 with respect to a lipid bilayer. (B) X-band DEER time domain data at 80 K for C99 that was spin-labeled at the ends of its TMD (at sites 700 and 723). Data are shown for WT C99 and also C99 that was additionally subjected to Gly-to-Leu mutations at G708 and G709. (C) Distance distributions between the spin labels measured for the corresponding time domain data. The error associated with each average distance relates to the uncertainty of the average. (Adapted from ref. 105 with permission)

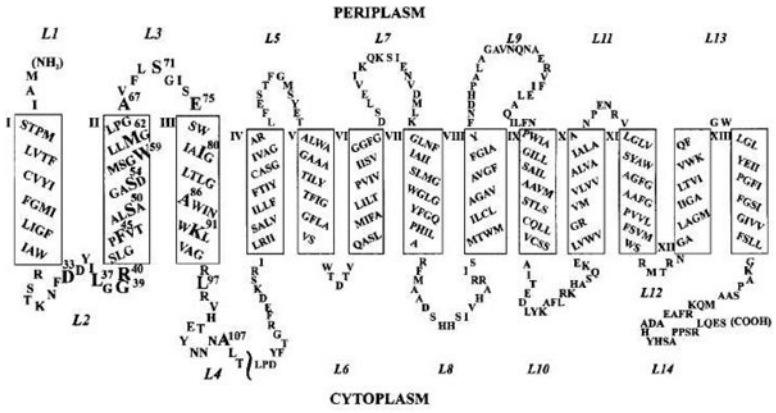

Figure 10.

Secondary structure model of Na^+/Proline Transporter PutP of E. coli. Putative TMs are represented as rectangles and numbered with Roman numerals; loops are numbered with Arabic numerals starting from the N-terminus. (Adapted from ref. 110 with permission)

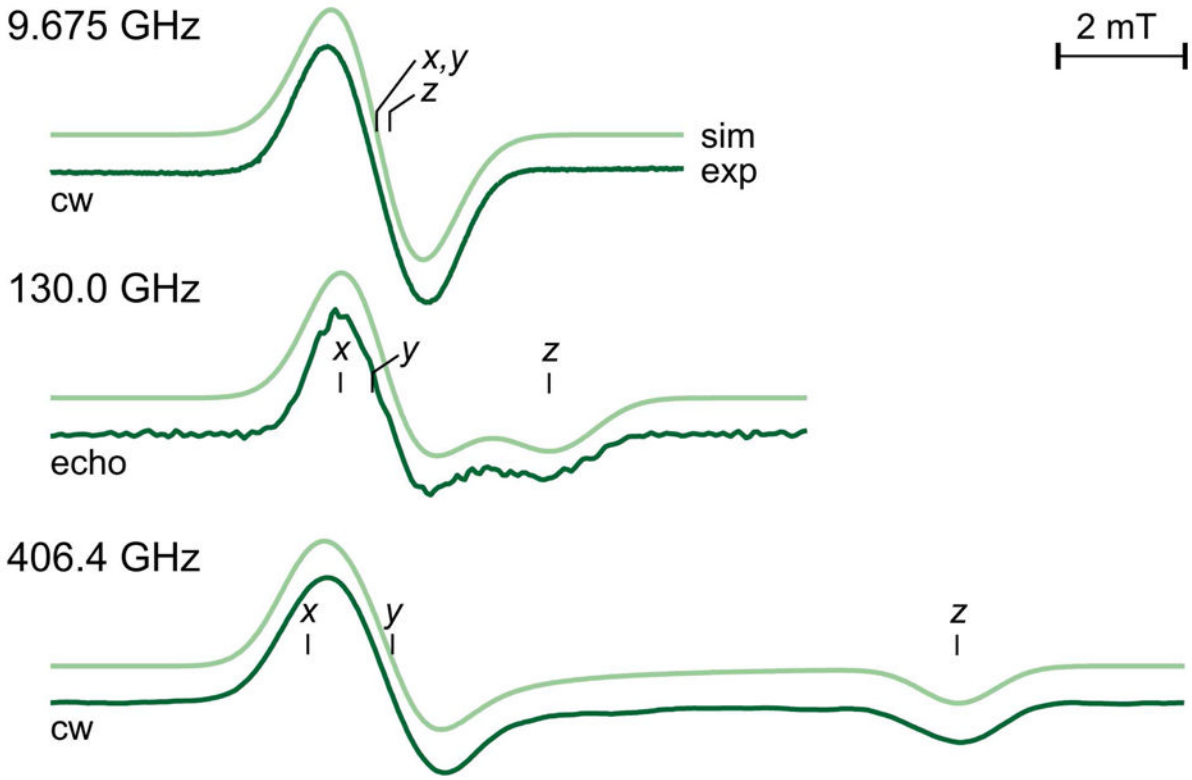

Figure 11.
EPR spectra and corresponding simulations at three fields/frequencies of the radical intermediate in the Phycocyanobilin–Ferredoxin Oxidoreductase system. As the frequency increases, what is an isotropic signal at X-band eventually becomes much better resolved allowing for the determination of all three g values. Reproduced with permission from reference 119.

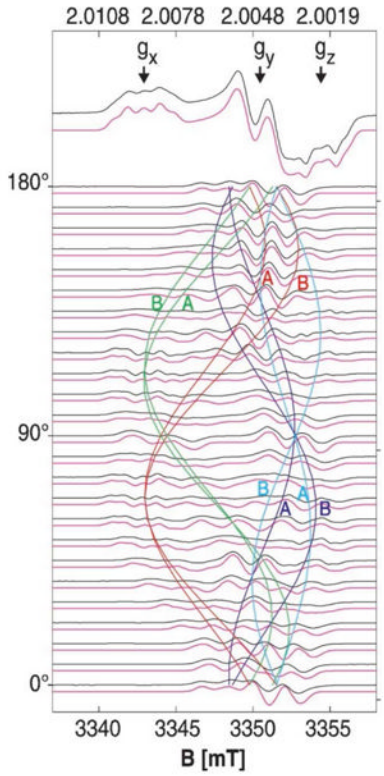

Figure 12.

These data show the single crystal rotation of the H_2O_2-induced tyrosine radical intermediate in ribonucleotide reductase. From the results, the researchers were able to determine the orientation of the tyrosine sidechain within the crystal, which is slightly rotated from X-ray diffraction structure of the resting state. Reproduced with permission from reference 127.

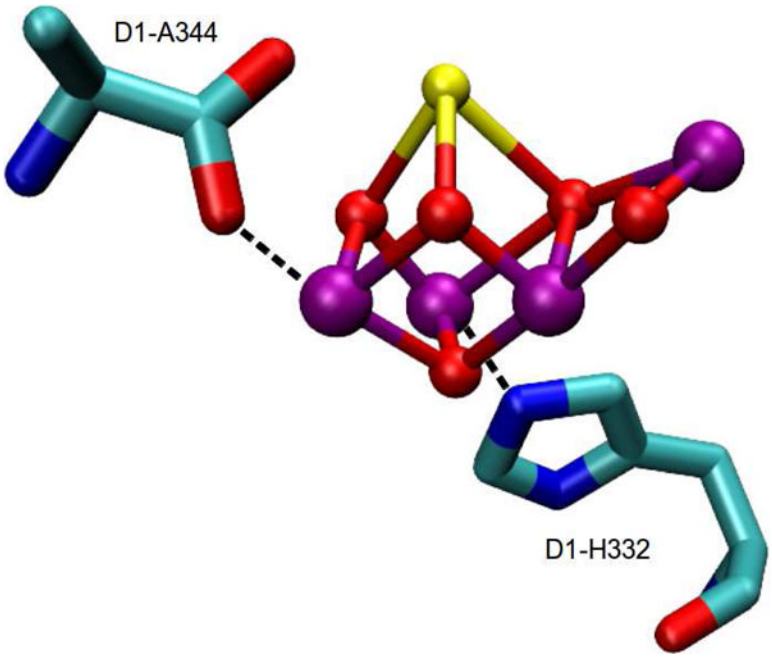

Figure 13.
X-ray crystal structure of metalloenzyme core of the oxygen evolving complex (OEC) (PDB ID: 3ARC).[133] Atoms are shown in the following colors: Mn, purple; Ca, yellow; O, red. The figure was prepared using VMD.[50]

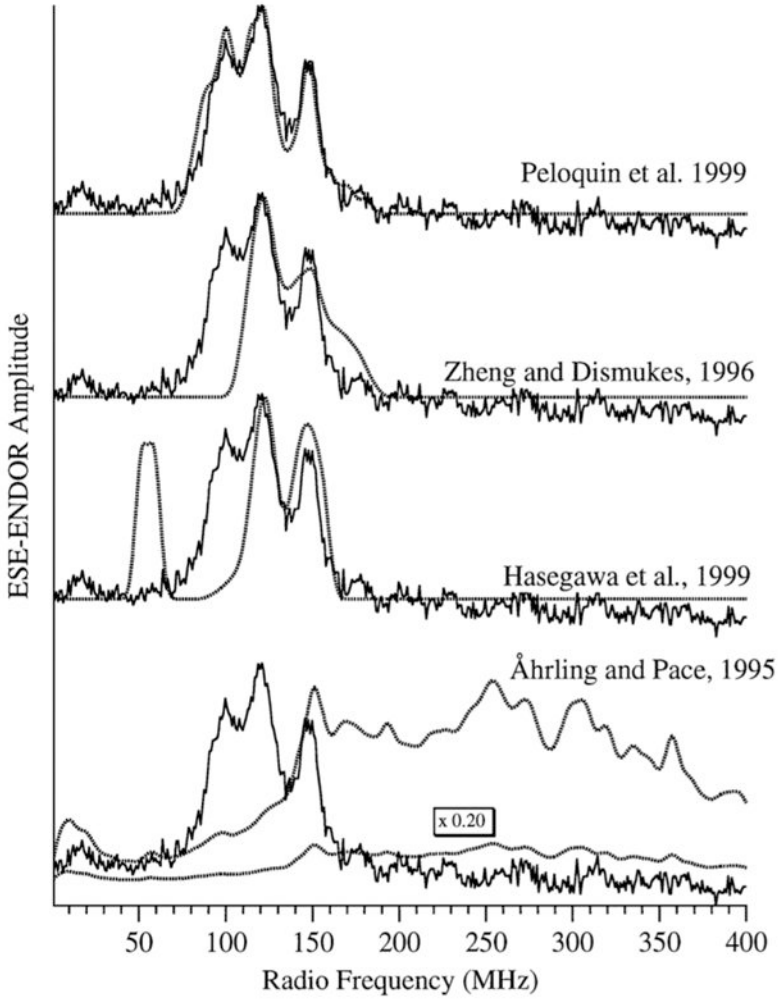

Figure 14.

Shown in this figure are the ^{55}Mn ESE ENDOR data collected by the Britt laboratory and the corresponding simulations using the hyperfine parameters from various predictions based on the multiline signal. The utility of using combined EPR methods is apparent as each of these sets of parameters can adequately simulate the multiline EPR signal in the S_2 state of the OEC, only the Britt values can be used to adequately simulate the ^{55}Mn ESE ENDOR spectrum. Reproduced with permission from reference 147.

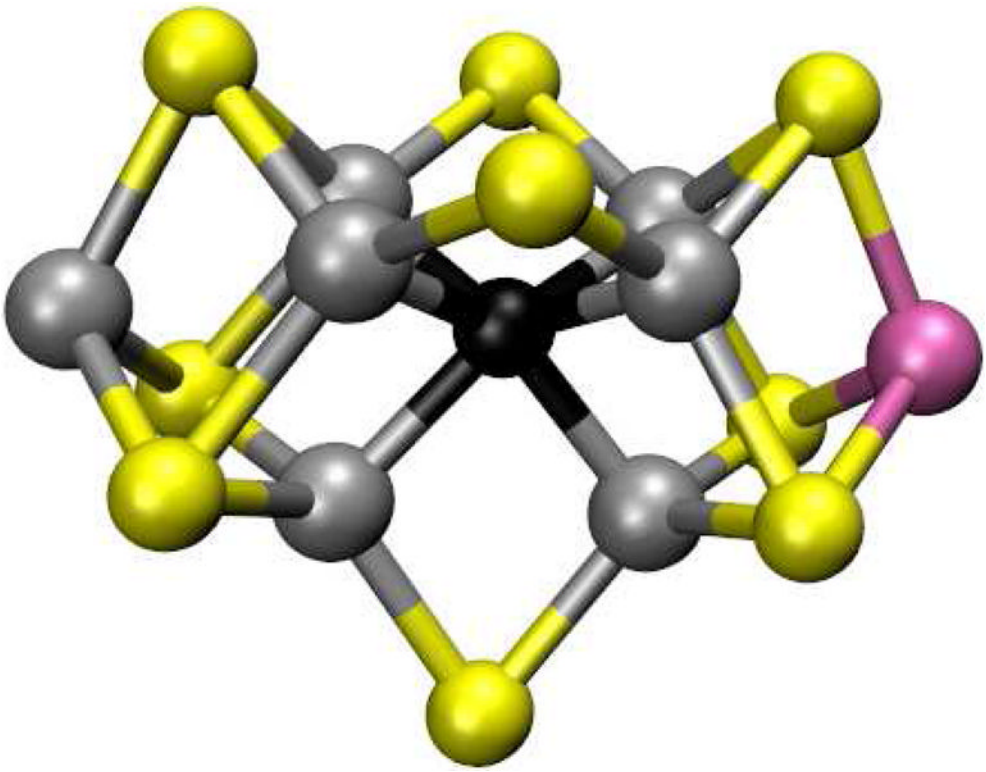

Figure 15.
X-ray crystal structure of FeMo cofactor of Nitrogenase (PDB ID: 3U7Q).[163] Atoms are shown in the following colors: Mo, magenta; Fe, silver; S, yellow; Interstitial light atom, black. The figure was prepared using VMD.[50]

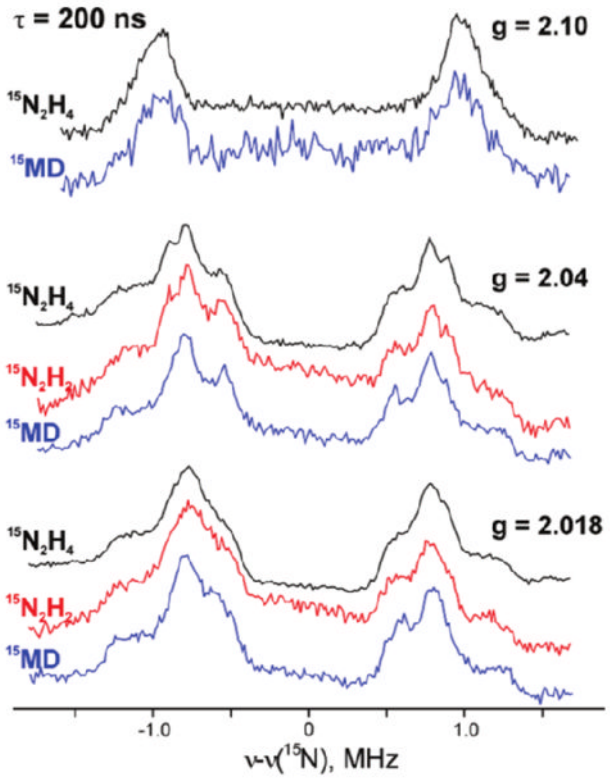

Figure 16.

^{15}N ReMims ENDOR spectra of a trapped intermediate state in the Nitrogenase enzyme with $^{15}N_2H_4$, $^{15}N_2H_2$ or $^{15}N{=}N{-}CH_3$ (MD). The data show a single intermediate common to each of the added substrates. Adapted with permission from reference 167.